Received 16 August 2020; revised 16 September 2020; accepted 25 September 2020. Date of publication 7 October 2020; date of current version 30 October 2020. The review of this article was arranged by Associate Editor Eric Monmasson.

Digital Object Identifier 10.1109/OJIES.2020.3029358

Enabling Multistep Model Predictive Control for Transient Operation of Power Converters

ROKY BAIDYA [1] (Member, IEEE), RICARDO P. AGUILERA [1] (Member, IEEE), PABLO ACUÑA [2] (Member, IEEE), TOBIAS GEYER [3] (Senior Member, IEEE), RAMÓN A. DELGADO [4], DANIEL E. QUEVEDO [5] (Senior Member, IEEE), AND HENDRIK DU TOIT MOUTON [6] (Member, IEEE)

[1]School of Electrical and Data Engineering, University of Technology Sydney (UTS), Sydney, NSW 2007, Australia
[2]Department of Electrical Engineering, Universidad de Talca, Curicó, Talca 334000, Chile
[3]ABB Medium-Voltage Drives, 5300 Turgi, Switzerland
[4]School of Electrical Engineering and Computing, University of Newcastle, Callaghan, NSW 2308, Australia
[5]School of Electrical Engineering & Robotics (EER), Queensland University of Technology, Brisbane, QLD 4000, Australia
[6]Department of Electrical and Electronic Engineering, Stellenbosch University, Stellenbosch 7599, South Africa

CORRESPONDING AUTHOR: ROKY BAIDYA (e-mail: rokybaidya@gmail.com)

This work was supported in part by the Australian Government through the Australian Research Council (Discovery Project No. DP180100129) and in part by CONICYT + FONDECYT Regular + 1191520.

ABSTRACT Recently, an efficient multistep direct model predictive control (MPC) scheme for power converters has been proposed. It relies on the Sphere Decoding Algorithm (SDA) to solve the associated long-horizon optimal control problem. Since the SDA evaluates only a small number of candidate solutions to find the optimal one, a significant reduction in the average computational burden can be achieved compared to the basic exhaustive search approach. However, this is only true during steady-state operation. In fact, the SDA still requires a large execution time during transients. This paper shows that if not properly addressed, the dynamic performance of the system may be degraded, which clearly limits its practical application. To mitigate this issue, which particularly arises during transients, an efficient preconditioning approach for the SDA is proposed. This approach ensures that only a small number of candidate solutions are evaluated during both steady-state, and transients. This allows the multistep direct MPC to become a viable control alternative for power converters operating at low semiconductor switching frequencies, e.g., below 450 Hz. The proposal is validated using a grid-connected three-level converter as a case study. Both processor-in-the-loop simulations, and experimental results on a scaled-down 2.24 kVA laboratory setup are presented.

INDEX TERMS Convex hull, integer least squares problem, model predictive control, power converters, quadratic programming solver, sphere decoding algorithm.

I. INTRODUCTION

Direct model predictive control (MPC) takes advantage of the power converter switching nature by directly considering the combinations of power switch states or output voltage levels as the manipulable system input. An optimal control problem is formulated to determine the input to be applied to the system. This considers a cost function and a prediction model that forecast the future system behavior over a finite prediction horizon. Finally, the optimal control input is usually found by evaluating all the possible input combinations in the cost function. The input that provides the minimum cost is, thus, the optimal one. This basic optimization process is referred to as the exhaustive search algorithm (ESA) [1]. However, using the basic ESA to solve the associated optimal control problem over a prediction horizon of more than one step (commonly known as multistep MPC) leads to a high computational burden since the total number of input combinations increases exponentially. To address this issue, it was recently shown that the sphere decoding algorithm (SDA), as in [2], can be adopted to efficiently solve the optimal control problem associated with multistep direct MPC schemes [3]. In that case, an improved steady-state performance is observed [4]–[7]. Compared to the basic single-step predictive approaches, the multistep MPC offers reduced voltage and current

This work is licensed under a Creative Commons Attribution 4.0 License. For more information, see https://creativecommons.org/licenses/by/4.0/

distortions and/or very low switching frequencies. Furthermore, as demonstrated in [4], the total harmonic distortion of the current is significantly reduced when compared with a space vector modulation for long prediction horizons and a low switching frequency. For that reason, the practical potentiality of multistep MPC has an increasing value in medium/high power converter applications at low switching frequencies.

In essence, the SDA is a branch-and-bound search technique that solves an integer least-squares (ILS) problem, which is indeed a reformulation of the associated optimization problem [2], [8]. To do this, an initial sphere in the input space is defined considering the, so-called, unconstrained optimal input as center. The size of this initial sphere is determined by the radius formed between this center and an initial input candidate. If properly chosen, a large number of candidate (input) solutions are discarded in the subsequent search process. Therefore, a significant reduction in the computational burden can be achieved compared to the basic ESA. Recently, to further reduce the computational burden, a modification in the ILS-problem using a lattice reduction algorithm [9] and refinement in the SDA has been proposed in [10]. These refinements in the branching and reverse-tracking procedures of the SDA lead to a reduction in the computational complexity of more than 55% compared to the one in [4]. Additionally, in [11], a shorter time to execute the SDA by limiting the number of computations to be performed has been achieved. This method guarantees the termination of the computation process within the defined sampling interval, but at the occasional expense of yielding a sub-optimal solution. In an industrial automotive application [6], a multistep MPC offers 40% reduction in the computational complexity for a prediction horizon length of four. This is achieved by reversing the temporal arrangement of the control input vector. Therefore, the ILS-problem can be solved in a backwards manner, which requires less algebraic manipulations in a real-time implementation.

Despite all the efforts put into reducing the computational burden of SDA, there is still a key problem that may affect the real-time implementation with long prediction horizons: the operation of multistep direct MPC during transients. When a change in the power converter reference is introduced, the initial radius of the SDA can become extremely large, yielding a high computational burden. This is a crucial issue since power converters often operate in transient conditions due to reference changes (current, voltage, power, torque, speed, etc.) or simply to compensate external disturbances (voltage sags, voltage swells, etc.). Due to the high computational burden during transients, a real-time implementation can be restricted to short prediction horizon such as one to three only. This clearly limits the applicability of multistep direct MPC to power electronics applications for higher prediction horizons. To address this problem, this work proposes an efficient preconditioning approach for the SDA. This approach consists of optimally obtaining a new initial center and a feasible initial candidate solution close to it. Thus, a small initial radius is always obtained, ensuring that only a small number of candidate solutions is evaluated during both steady-state and transients. Hence, the execution time will remain within the sampling interval limit for a selected prediction horizon, enabling the real-time implementation of direct MPC with long prediction horizons. This allows multistep direct MPC to become a viable control alternative for power converters.

The previously discussed idea of obtaining a new initial sphere center to address the computational burden of SDA during transients was originally proposed in the preliminary work [12]. Afterwards, this idea has been adopted in [13] for a multistep MPC formulated as in [10], with simulations results on a variable speed drive system. Subsequently, a deterministic use of multistep MPC under several drive system conditions has been evaluated in a three-level induction machine drive switching at 350 Hz [14]. The paper at hand extends the work in [12] by considering a generic control formulation for a power converter system (modeled as a linear system with quantized inputs), a detailed computational analysis, and a geometric optimality interpretation. Moreover, a grid-connected three-phase three-level H-Bridge (HB) converter as a case study is presented with the processor-in-the-loop (PIL) simulations for performance evaluation with different prediction horizons, and an optimality analysis with experimental verifications. The impact of transient operation on the computational burden is compared with the standard SDA initialization [3] and also with the approach in which a limited number of computations in the SDA is allowed [11].

II. MULTISTEP MPC FOR POWER CONVERTERS

This section introduces the optimal control problem of interest in a multistep direct MPC formulation for power converters. Firstly, it is assumed that the power converter and load can be modeled in discrete-time via

$$\boldsymbol{x}(k+1) = \boldsymbol{A}\boldsymbol{x}(k) + \boldsymbol{B}\boldsymbol{u}(k) \tag{1a}$$

$$\boldsymbol{y}(k) = \boldsymbol{C}\boldsymbol{x}(k) \tag{1b}$$

where $\boldsymbol{x} \in \mathbb{R}^{n_x}$ stands for the state vector with n_x-system state variables (e.g., currents, voltages, torques, etc.), and $\boldsymbol{y} \in \mathbb{R}^{n_y}$ the output vector with n_y-system outputs to be controlled. A distinguishing feature of direct MPC is that the control input vector, $\boldsymbol{u}$, with n_u-control inputs (e.g., switch positions or output voltage levels) belongs to a finite control set (FCS), $\boldsymbol{u} \in \mathbb{V}^{n_u}$, where

$$\mathbb{V} = \{u_{\min}, \ldots, u_{\max}\} \subset \mathbb{Z}. \tag{2}$$

Each element in $\boldsymbol{u}$ satisfies the constraint $u_{\min} \leq u_j \leq u_{\max}$, for all $j \in \{1, \ldots, n_u\}$. Generally, the main control target in a predictive control formulation is to track the desired output references, $\boldsymbol{y}^\star \in \mathbb{R}^{n_y}$, (i.e., $\boldsymbol{y} \to \boldsymbol{y}^\star$) [1]. Additional targets can be included, such as switching effort minimization, capacitor voltage balancing, common-mode voltage (CMV) reduction, imposed load-current spectrum etc. [15]–[18]. Recently, a direct MPC formulation that tracks a control input reference, $\boldsymbol{u}^\star$, (i.e., $\boldsymbol{u} \to \boldsymbol{u}^\star$), in addition to the output reference, has been

proposed in [19]. This has the advantage of achieving almost-symmetric output voltages, which helps to reduce the CMV and evenly distribute the power losses in each phase. Moreover, this direct MPC formulation can also be used to guarantee stability of this MPC class in power electronics [20], achieve inter-phase power balance [21], and formulate a selective harmonic elimination MPC strategy [22]. Based on this, a quadratic cost function over a finite prediction horizon, N, can be written as

$$J(k) = \sum_{l=k}^{k+N-1} \|\boldsymbol{y}(\ell+1) - \boldsymbol{y}^\star(\ell+1)\|_2^2 + \sigma\|\boldsymbol{u}(l) - \boldsymbol{u}^\star(l)\|_2^2 \tag{3}$$

where both tracking terms are presented as the quadratic Euclidean norm, i.e., $\|\boldsymbol{m} - \boldsymbol{m}^\star\|_2^2 = (m_1 - m_1^\star)^2 + \cdots + (m_n - m_n^\star)^2$, for $\boldsymbol{m} = \{\boldsymbol{y}, \boldsymbol{u}\}$ and $\boldsymbol{m}^\star = \{\boldsymbol{y}^\star, \boldsymbol{u}^\star\}$. In (3), the weighting factor, σ, is designed to give relative importance to the input over the output tracking error in order to obtain a desired steady-state behavior [19], [21], [22]. To maintain the fast dynamic nature of direct MPC, a smaller value for σ must be chosen, see [19].

At every time-step k, the optimal control input sequence

$$\boldsymbol{U}_{\text{opt}}(k) = [\boldsymbol{u}_{\text{opt}}{}^T(k) \ldots \boldsymbol{u}_{\text{opt}}{}^T(k+N-1)]^T \tag{4}$$

is obtained by solving the following original optimization problem

$$\boldsymbol{U}_{\text{opt}}(k) = \arg\min_{\boldsymbol{U}(k)} \{J(k)\} \tag{5a}$$

$$\text{subj. to: } \boldsymbol{x}(\ell+1) = \boldsymbol{A}\boldsymbol{x}(\ell) + \boldsymbol{B}\boldsymbol{u}(\ell) \tag{5b}$$

$$\boldsymbol{y}(\ell) = \boldsymbol{C}\boldsymbol{x}(\ell) \tag{5c}$$

$$\boldsymbol{U}(k) \in \mathbb{U} = \mathbb{V}^\zeta, \text{ with } \zeta = n_u N \tag{5d}$$

$$\|\Delta\boldsymbol{u}(\ell)\|_\infty \leq 1, \ \forall \ell = k, \ldots, k+N-1 \tag{5e}$$

where $\Delta\boldsymbol{u}(\ell) = \boldsymbol{u}(\ell) - \boldsymbol{u}(\ell-1)$. Here, (5b) and (5c) refers to the system model given in (1). Then, (5d) restricts the control input sequence, $\boldsymbol{U}(k) = [\boldsymbol{u}^T(k) \ldots \boldsymbol{u}^T(k+N-1)]^T$, to the FCS, Furthermore, (5e) is the transition voltage level constraint that in high-power multilevel converters, is usually limited to one to avoid an excessive dv/dt [1]. Note that such large transition voltage levels (more than one) tend to appear during transients. Following the receding horizon policy, only the first element of $\boldsymbol{U}_{\text{opt}}(k)$ in (4) is applied to the converter. This process is repeated with fresh measurements at every time-step k. It is worth emphasizing that despite the fact that only its first element is applied, each pair of time-consecutive vectors in (4) satisfies the constraint (5e).

III. SDA-BASED OPTIMIZATION PROCESS

To solve the optimization problem in (5), the SDA as presented in [3], [19] is adopted as a computationally efficient alternative to the standard ESA.

A. OPTIMIZATION PROBLEM REFORMULATION

The SDA efficiently obtains $\boldsymbol{U}_{\text{opt}}(k)$ by transforming the original optimization problem (5) into an equivalent ILS-problem. Firstly, the cost function (3) is rewritten as a convex quadratic function of $\boldsymbol{U}(k)$, i.e.,

$$J(k) = \boldsymbol{U}(k)^T\boldsymbol{W}\boldsymbol{U}(k) + 2\boldsymbol{F}^T(k)\boldsymbol{U}(k) + \boldsymbol{\varepsilon}(k) \tag{6}$$

where

$$\boldsymbol{W} = \boldsymbol{\Phi}^T\boldsymbol{\Phi} + \sigma\boldsymbol{I}_{\zeta\times\zeta} \tag{7a}$$

$$\boldsymbol{F}(k) = \boldsymbol{\Phi}^T\boldsymbol{\Lambda}\boldsymbol{x}(k) - \boldsymbol{\Phi}^T\boldsymbol{Y}^\star(k) - \sigma\boldsymbol{U}^\star(k). \tag{7b}$$

Here, $\boldsymbol{\varepsilon}(k)$ is independent on $\boldsymbol{U}(k)$ and, thus, discarded from the subsequent formulation. The vectors $\boldsymbol{Y}^\star(k) = [(\boldsymbol{y}^\star(k+1))^T \ldots (\boldsymbol{y}^\star(k+N))^T]^T$ and $\boldsymbol{U}^\star(k) = [(\boldsymbol{u}^\star(k))^T \ldots (\boldsymbol{u}^\star(k+N-1))^T]^T$ are the output and control input sequence references, respectively. Furthermore, $\boldsymbol{I}_{\zeta\times\zeta}$ is the ζ-dimensional identity matrix. The matrices $\boldsymbol{\Phi}$ and $\boldsymbol{\Lambda}$ are given as

$$\boldsymbol{\Phi} = \begin{bmatrix} \boldsymbol{CB} & \boldsymbol{0} & \ldots & \boldsymbol{0} & \boldsymbol{0} \\ \boldsymbol{CAB} & \boldsymbol{CB} & \ldots & \boldsymbol{0} & \boldsymbol{0} \\ \vdots & \vdots & \ddots & \vdots & \vdots \\ \boldsymbol{CA}^{N-1}\boldsymbol{B} & \boldsymbol{CA}^{N-2}\boldsymbol{B} & \ldots & \boldsymbol{CAB} & \boldsymbol{CB} \end{bmatrix}$$

$$\boldsymbol{\Lambda} = \begin{bmatrix} \boldsymbol{CA} \\ \boldsymbol{CA}^2 \\ \vdots \\ \boldsymbol{CA}^N \end{bmatrix}.$$

Secondly, considering the real valued control input sequence, i.e., $\boldsymbol{U}(k) \in \mathbb{R}^\zeta$, the unconstrained solution $\boldsymbol{U}_{\text{uc}}(k)$ to the optimization problem (5) is given by

$$\boldsymbol{U}_{\text{uc}}(k) = \arg\min_{\boldsymbol{U}(k)\in\mathbb{R}^\zeta} \{J(k)\} = -\boldsymbol{W}^{-1}\boldsymbol{F}(k). \tag{9}$$

As shown in [3], a non-singular lower triangular matrix, $\boldsymbol{H} \in \mathbb{R}^{\zeta\times\zeta}$, known as lattice generator matrix, can be obtained from the symmetric and positive definite matrix $\boldsymbol{W}$ (for $\sigma > 0$), by using the Cholesky decomposition [23], leading to $\boldsymbol{W} = \boldsymbol{H}^T\boldsymbol{H}$. Finally, conducting some algebraic manipulations, the original problem in (5) is transformed into the following ILS-problem

$$\boldsymbol{U}_{\text{opt}}(k) = \arg\min_{\boldsymbol{U}(k)} \|\boldsymbol{H}\boldsymbol{U}(k) - \bar{\boldsymbol{U}}_{\text{uc}}(k)\|_2^2 \tag{10}$$

subject to (5d) and (5e), with $\bar{\boldsymbol{U}}_{\text{uc}} = \boldsymbol{H}\boldsymbol{U}_{\text{uc}}$. Importantly, a new transformed space (contains all $\boldsymbol{HU}$) is formed by the lattice generator matrix $\boldsymbol{H}$, where the SDA will perform the optimization to find $\boldsymbol{U}_{\text{opt}}$ as per (10). Once the ILS-problem in (10) has been formed, the next step is to initialize the SDA.

B. STANDARD INITIALIZATION OF SDA

To start the SDA, it is required to define an initial sphere in the new transformed space. This sphere is set by considering $\boldsymbol{\Theta}(k) = \bar{\boldsymbol{U}}_{\text{uc}}(k)$ as a center and by choosing an initial control

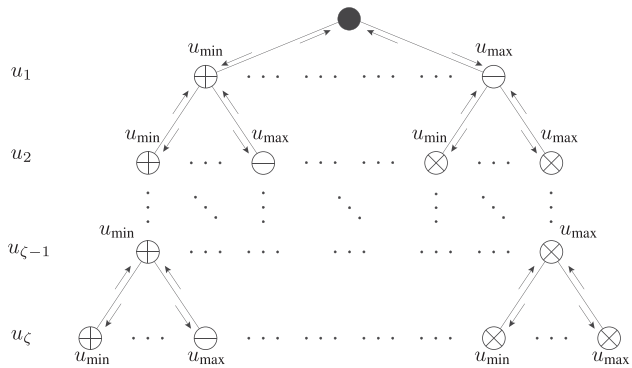

FIGURE 1. A tree-diagram of the control input sequence $U \in \mathbb{U}$ that illustrates the evaluation process of nodes in the SDA. The evaluated nodes that belong and do not belong to the incumbent sphere $\mathcal{S}_{inc}$ are shown as $\oplus$ and $\ominus$, respectively. Here, $\otimes$ represents the unevaluated nodes. By visiting nodes from left to right (i.e., u_{min} to u_{max}), the evaluation process advances from top to bottom (i.e., $i = 1$ to ζ) and also includes reverse-tracking, as indicated by arrows.

input sequence candidate $\boldsymbol{U}_{\text{ini}}(k)$ which determines its initial radius, $\rho_{\text{ini}}(k)$, i.e.,

$$\mathcal{S}_{\text{ini}} = \left\{\boldsymbol{U}_{\text{ini}}(k) : \rho^2_{\text{ini}}(k) = \|\boldsymbol{H}\boldsymbol{U}_{\text{ini}}(k) - \boldsymbol{\Theta}(k)\|_2^2\right\}. \quad (11)$$

This initial sphere $\mathcal{S}_{\text{ini}}$ should be small enough containing as few candidate solutions as possible, but should not be empty. In [3], the initial control input sequence is chosen by considering an educated-guess, $\boldsymbol{U}_{\text{ini}}(k) = \boldsymbol{U}_{\text{eg}}(k)$, based on the previous optimal input sequence, $\boldsymbol{U}_{\text{opt}}(k-1)$, and extending it by one time-step, i.e.,

$$\boldsymbol{U}_{\text{eg}}(k) = \begin{bmatrix} \boldsymbol{0}_{n_u} & \boldsymbol{I}_{n_u} & \boldsymbol{0}_{n_u} & \dots & \boldsymbol{0}_{n_u} \\ \boldsymbol{0}_{n_u} & \boldsymbol{0}_{n_u} & \boldsymbol{I}_{n_u} & \dots & \boldsymbol{0}_{n_u} \\ \vdots & \ddots & \vdots & \ddots & \vdots \\ \boldsymbol{0}_{n_u} & \dots & \boldsymbol{0}_{n_u} & \dots & \boldsymbol{I}_{n_u} \\ \boldsymbol{0}_{n_u} & \dots & \boldsymbol{0}_{n_u} & \dots & \boldsymbol{I}_{n_u} \end{bmatrix} \boldsymbol{U}_{\text{opt}}(k-1) \quad (12)$$

where $\boldsymbol{I}_{n_u}$ and $\boldsymbol{0}_{n_u}$ are the identity and zero matrices of size n_u (number of control inputs), respectively. Thus, using $\boldsymbol{U}_{\text{eg}}$ and $\bar{\boldsymbol{U}}_{\text{uc}}$ the initial sphere $\mathcal{S}_{\text{ini}}$ in (11) becomes

$$\mathcal{S}_{\text{eg}} = \left\{\boldsymbol{U}_{\text{eg}}(k) : \rho^2_{\text{eg}}(k) = \|\boldsymbol{H}\boldsymbol{U}_{\text{eg}}(k) - \bar{\boldsymbol{U}}_{\text{uc}}(k)\|_2^2\right\}. \quad (13)$$

This initialization method, i.e., $\rho_{\text{ini}} = \rho_{\text{eg}}$, is particularly suitable for steady-state operation, since it exploits the receding horizon policy in MPC, and $\boldsymbol{U}_{\text{eg}}$ satisfies the constraints in (5d) and (5e).

C. FINDING THE OPTIMAL SOLUTION

The iterative optimization process in the SDA begins by considering $\boldsymbol{U}_{\text{ini}}$ as the initial incumbent[1] solution, i.e., $\boldsymbol{U}_{\text{inc}} = \boldsymbol{U}_{\text{ini}}$, and also $\rho_{\text{inc}} = \rho_{\text{ini}}$, thus, the incumbent initial sphere $\mathcal{S}_{\text{inc}} = \mathcal{S}_{ini}$. Then, a tentative solution, $\tilde{\boldsymbol{U}} = \left[u_1 \dots u_i \dots u_\zeta\right]^T \in \mathbb{U}$, is constructed (element by element)

[1]The term incumbent is used to denote the so far best feasible solution in the iterative optimization process of the SDA.

Algorithm 1: SDA-Based Optimization.

$\boldsymbol{U}_{\text{inc}} \leftarrow \boldsymbol{U}_{\text{ini}}$ and $\rho_{\text{inc}} \leftarrow \rho_{\text{ini}}$
function $[\boldsymbol{U}_{\text{opt}}] = \text{SDA}\ (\boldsymbol{H}, \boldsymbol{\Theta}, \boldsymbol{U}_{\text{inc}}, \rho_{\text{inc}})$
For each $u_i \in \mathbb{V}$, where $i \in \{1, 2, \dots, \zeta\}$**do**
  $\tilde{\boldsymbol{U}}_{[1,i]} \leftarrow u_i$
  $\rho_i^2 \leftarrow \|\boldsymbol{H}_{[i,1:i]}\tilde{\boldsymbol{U}}_{[1:i]} - \Theta_i\|_2^2 + \rho^2_{i-1}$ ▷ see (14)
  if $\rho_i \leqslant \rho_{\text{inc}}$**then** ▷ see (15)
    if $i < \zeta$ **then** $i = i + 1$
      $\text{SDA}(\boldsymbol{H}, \boldsymbol{\Theta}, \boldsymbol{U}_{\text{inc}}, \rho_{\text{inc}})$
    else ▷ when $i = \zeta$
      if $\tilde{\boldsymbol{U}}$ meets (5e)**then**
        $\boldsymbol{U}_{\text{inc}} \leftarrow \tilde{\boldsymbol{U}}$ and $\rho_{\text{inc}} \leftarrow \rho_\zeta$
      end if
    end if
  end if
end for
$\boldsymbol{U}_{\text{opt}} \leftarrow \boldsymbol{U}_{\text{inc}}$
end function

by performing element-wise computations[2]. This process is illustrated with a tree-diagram of $\boldsymbol{U}$ in Fig. 1, where each element $u_i \in \mathbb{V}$ is called a node. Additionally, a pseudocode in Algorithm 1 presents the iterative computational steps involves in solving the ILS-problem of type (10). Starting from $i = 1$ and considering (10), a tentative value for u_i from $\mathbb{V}$ is accepted (or discarded) by evaluating the following partial radius

$$\rho_i^2 = \|\underbrace{[h_{i1} \dots h_{ii}]}_{\boldsymbol{H}_{[i,1:i]}}\underbrace{[u_1 \dots u_i]^T}_{\tilde{\boldsymbol{U}}_{[1:i]}} - \bar{u}_{\text{uc},i}\|_2^2 + \rho^2_{i-1} \quad (14)$$

where $\rho_0 = 0$. If the evaluated node u_i satisfies

$$\rho_i^2 \leq \rho^2_{\text{inc}} \quad (15)$$

then, it is denoted as $\oplus$, and the algorithm proceeds toward the next node u_{i+1}. Notice that as i increases, the size of the partially formed tentative vector $\tilde{\boldsymbol{U}}_{[1:i]}$ is also increased. In contrast, if a particular node u_i does not satisfy (15), it is then denoted as $\ominus$. This violation implies that any $\boldsymbol{U} \in \mathbb{U}$ starts with $\tilde{\boldsymbol{U}}_{[1:i]}$ will lie outside $\mathcal{S}_{\text{inc}}$, since it will generate a radius larger than ρ_{inc}, and thus, there is no need to evaluate it. Therefore, for each u_i ($\ominus$), the SDA discards all following nodes (from u_{i+1} to u_ζ) from being evaluated—whose are symbolized with $\otimes$. Moreover, once the algorithm finds a node u_i of type $\ominus$, it reverses the formation of tentative vector $\tilde{\boldsymbol{U}}$, i.e, $\tilde{\boldsymbol{U}}_{[i-1:1]}$, by searching any unvisited nodes. This process is called reverse-tracking. Proceeding in this manner, whenever a tentative vector is fully formed, i.e., $\tilde{\boldsymbol{U}} = \tilde{\boldsymbol{U}}_{[1:\zeta]}$, it is considered to be the new incumbent solution $\boldsymbol{U}_{\text{inc}}$ since its radius is smaller than ρ_{inc}. Consequently, $\boldsymbol{U}_{\text{inc}}$ and ρ_{inc} are updated with $\tilde{\boldsymbol{U}}$ and its corresponding radius ρ_ζ, respectively. Hence, a new smaller $\mathcal{S}_{\text{inc}}$ is found which further reduces

[2]Here, the index notation i denotes the position-number of an element in $\tilde{\boldsymbol{U}}$, and belongs to the set $\mathcal{Z} = \{1, 2, \dots, \zeta - 1, \zeta\} \subset \mathbb{Z}^+$. Throughout the paper, i is used as common notation for all other vectors.

the computations [3]. This process is continued until $\mathcal{S}_{\text{inc}}$ is reduced to a point that contains only one $\boldsymbol{U}_{\text{inc}}$, which is indeed the optimal solution $\boldsymbol{U}_{\text{opt}}$ in (10).

IV. COMPUTATIONAL BURDEN ANALYSIS

Based on the theoretical aspect in Section III, the computational burden of SDA during both steady-state and transient operation of a power converter is analyzed in this section.

This analysis is focused on the initial radius ρ_{ini}, and the total number of evaluated nodes, $\mathcal{N}_{\text{ev}}$, at each sampling instant, which can be expressed by

$$\mathcal{N}_{\text{ev}} = \sum_{i=1}^{\zeta} (n_i^{\text{cp}} + n_i^{\text{cm}}). \tag{16}$$

Here, n_i^{cp} and n_i^{cm} refer to the number of $\oplus$ and $\ominus$ at i^{th} dimension of $\boldsymbol{U}$ (i.e., U_i, where $i \in \mathcal{Z}$). As one can understand from Section III-C that the SDA runs through the calculation (14) and the condition (15), each time a node u_i ($\oplus$ and/or $\ominus$) is visited. If properly selected, ρ_{ini} will be relatively small. Then, based on (14), the partial radius ρ_i formed by $\tilde{\boldsymbol{U}}_{[1,i]}$ will be smaller than ρ_{inc} only for small values of i, i.e., $i \approx 1$. Hence, a larger number of nodes will be discarded from calculations leading to a small $\mathcal{N}_{\text{ev}}$. Conversely, a larger value of ρ_{ini} may lead to a considerably high $\mathcal{N}_{\text{ev}}$. Hence, the total number of calculations to be performed is also increased. Notice that using (11), the initial radius size depends not only on the initial control input sequence $\boldsymbol{U}_{\text{ini}}$ but also on the sphere's center $\boldsymbol{\Theta}$. Since until now $\boldsymbol{\Theta}$ has been chosen based on the unconstrained optimal solution, i.e., $\boldsymbol{\Theta} = \bar{\boldsymbol{U}}_{\text{uc}}$, it is important to analyze its location in the input space during both steady-state and transients. To this end, it is convenient to bound the input space by the *Convex-Hull* $\mathbb{C}_{\mathcal{H}}$ of the FCS $\mathbb{U}$ [24], [25], which can be defined as

$$\mathbb{C}_{\mathcal{H}} = \mathbf{C}onv(\mathbb{U}) \subset \mathbb{R}^{\zeta}. \tag{17}$$

As per definition, $\mathbb{C}_{\mathcal{H}}$ is the smallest convex set in an ζ-dimensional space, where $\mathbb{U} \subset \mathbb{C}_{\mathcal{H}}$. Since each entry of $\mathbb{U}$ belongs to the set $\mathbb{V}$ in (2), $\mathbb{C}_{\mathcal{H}}$ is expected to satisfy the following bound-constraint of linear inequalities

$$\boldsymbol{U}_{\min} \preceq \mathbb{C}_{\mathcal{H}} \preceq \boldsymbol{U}_{\max} \tag{18}$$

where the lower bound vector $\boldsymbol{U}_{\min} = [u_{\min}, \ldots, u_{\min}]^T \subset \mathbb{Z}^{\zeta}$ and the upper bound vector $\boldsymbol{U}_{\max} = [u_{\max}, \ldots, u_{\max}]^T \subset \mathbb{Z}^{\zeta}$. The relational symbol $\preceq$ in (18) represents the element-wise inequality.

An illustration of the optimization process during a transient operation is depicted in Fig. 2. This example is shown for an FCS $\mathbb{U}$ of nine control input vectors (gray solid circles), which are formed with $\mathbb{V}$ of three elements, $n_u = 2$, $N = 1$, and thus $\zeta = 2$. Thus, the associated $\mathbb{C}_{\mathcal{H}}$ is depicted in Fig. 2 a. The ellipses centered in $\boldsymbol{U}_{\text{uc}}$ represent the level sets of the original optimization problem (10), i.e., all input combinations that belong to the same ellipse generate the same cost value. On the other hand, a bigger ellipse corresponds to a larger cost value. The matrix $\boldsymbol{H}$ in (10) introduces a

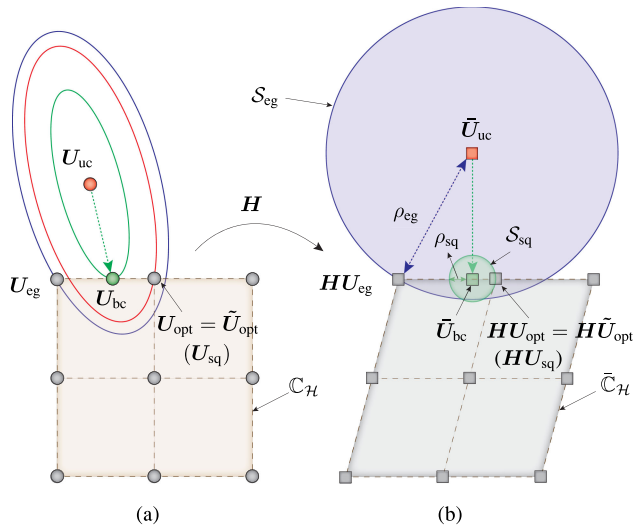

FIGURE 2. Graphical representation of the direct MPC problem (an FCS $\mathbb{U}$ of nine control input vectors) for transient operation, where both the standard and the proposed initialization of the SDA in two-dimensional space are considered. (a) Original space and (b) transformed space generated by $\boldsymbol{H}$.

linear transformation that generates a new transformed space in Fig. 2 b. In this space, the original ellipses are transformed into circles (spheres for larger dimensions) centered in $\bar{\boldsymbol{U}}_{\text{uc}} = \boldsymbol{H}\boldsymbol{U}_{\text{uc}}$. In fact, it is in this space where the SDA operates.

During steady-state operation, the system output $\boldsymbol{y}$ is close to its references, i.e., $\boldsymbol{y} \approx \boldsymbol{y}^{\star}$. This leads to an unconstrained solution $\boldsymbol{U}_{\text{uc}}$ that may be positioned near $\mathbb{C}_{\mathcal{H}}$, which, in turn, leads to an initial center $\boldsymbol{\Theta} = \bar{\boldsymbol{U}}_{\text{uc}}$ that may also be near $\bar{\mathbb{C}}_{\mathcal{H}} = \boldsymbol{H}\mathbb{C}_{\mathcal{H}}$. This, along with $\boldsymbol{U}_{\text{eg}}$, will result in a small initial radius $\rho_{\text{ini}} = \rho_{\text{eg}}$ as per (13), during steady-state operation and, thus a small number of evaluated $\mathcal{N}_{\text{ev}}$. On the other hand, during transients, the system output is far from its reference, i.e., $|\boldsymbol{y}| \gg |\boldsymbol{y}^{\star}|$. Therefore, a large actuation is required to lead it back to its reference. Since $\boldsymbol{U}_{\text{uc}}$ does not consider the converter limitations, it takes a large value that can place it far away from $\mathbb{C}_{\mathcal{H}}$, thus, $\boldsymbol{U}_{\text{uc}} \notin \mathbb{C}_{\mathcal{H}}$; see Fig. 2 a. In this situation, no matter what initial input $\boldsymbol{U}_{\text{ini}}$ is chosen, a large initial radius ρ_{ini} will be always obtained since its center $\boldsymbol{\Theta} = \bar{\boldsymbol{U}}_{\text{uc}}$ will be also far from $\bar{\mathbb{C}}_{\mathcal{H}}$; see Fig. 2 b. Moreover, using $\boldsymbol{U}_{\text{eg}}$ to compute ρ_{ini} is no longer a good guess during transients, since in this condition the new optimal solution, in general, totally differs from the previous one. As a result, a large number of nodes will be evaluated, which leads to an intractable large execution time T_e.

To overcome this problem, a computationally efficient preconditioning approach for the SDA is proposed next.

V. PROPOSED PRECONDITIONING APPROACH

The key idea of the proposed preconditioning approach is to transform the original optimal control problem into a form that is more suitable for the SDA during transients, see Remark 1 for generic detail. This approach consists of two parts: obtaining a new center $\boldsymbol{\Theta}$ and a new initial radius ρ_{ini}.

Algorithm 2: Box-Constrained QP Problem.

Input: $\boldsymbol{U}_{\text{uc}}$ in (9), when $\notin \mathbb{C}_{\mathcal{H}}$
Output: $\boldsymbol{U}_{\text{bc}}$ in (19), always $\in \mathbb{C}_{\mathcal{H}}$

Preliminaries

Lagrangian function for $\boldsymbol{U} \in \mathbb{R}^{\zeta}$:
1: $\mathcal{L}(\boldsymbol{U}, \boldsymbol{\xi}, \boldsymbol{\gamma}) =$
$\boldsymbol{U}^T\boldsymbol{W}\boldsymbol{U} + 2\boldsymbol{F}^T\boldsymbol{U} - \boldsymbol{\xi}(\boldsymbol{U} - \boldsymbol{U}_{\min}) - \boldsymbol{\gamma}(\boldsymbol{U}_{\max} - \boldsymbol{U})$.
Karush-Kuhn-Tucker (KKT) conditions at minimum $\boldsymbol{U}_{\text{bc}}, \boldsymbol{\xi}_{\text{bc}}, \boldsymbol{\gamma}_{\text{bc}}$:
2: $\nabla\mathcal{L} = \boldsymbol{W}\boldsymbol{U}_{\text{bc}} + \boldsymbol{F} - \boldsymbol{\xi}_{\text{bc}} + \boldsymbol{\gamma}_{\text{bc}} = \boldsymbol{0}$, and
3: $\xi_{\text{bc},i} \geq 0, \gamma_{\text{bc},i} \geq 0, \quad \forall i \in \mathcal{Z}$;
4: $\xi_{\text{bc},i}(U_{\text{bc},i} - U_{\min,i}) = 0, \quad \forall i \in \mathcal{Z}$;
5: $\gamma_{\text{bc},i}(U_{\max,i} - U_{\text{bc},i}) = 0, \quad \forall i \in \mathcal{Z}$;
6: $U_{\text{bc},i} \in [U_{\min,i}, U_{\max,i}], \quad \forall i \in \mathcal{Z}$.
The desired solution $\boldsymbol{U}_{bc}$ is obtained by following steps.

Step 1. Structure the sets

7: $\boldsymbol{S_l} = \{i : U_i < U_{\min,i}$, or $U_i = U_{\min,i}$ and $\xi_i \geq 0\}$.
8: $\boldsymbol{S_u} = \{i : U_i > U_{\max,i}$, or $U_i = U_{\max,i}$ and $\gamma_i \geq 0\}$.
9: $\boldsymbol{S_b} = \{i : U_{\min,i} < U_i < U_{\max,i}$, or $U_i =$
$U_{\min,i}$ and $\xi_i < 0$, or $U_i = U_{\max,i}$ and $\gamma_i < 0\}$.
Note that $\boldsymbol{S_l} \cup \boldsymbol{S_u} \cup \boldsymbol{S_b} = \mathcal{Z}$.

Step 2. Reset $\boldsymbol{U}, \boldsymbol{\xi}, \boldsymbol{\gamma}$ with boundary values

10: $U_i = U_{\min,i}, \gamma_i = 0, \quad \forall i \in \boldsymbol{S_l}$.
11: $U_i = U_{\max,i}, \xi_i = 0, \quad \forall i \in \boldsymbol{S_u}$.
12: $\xi_i = 0, \gamma_i = 0, \quad \forall i \in \boldsymbol{S_b}$.

Step 3. Reformation of $\boldsymbol{U}, \boldsymbol{\xi}, \boldsymbol{\gamma}$

13: Solve $\quad \boldsymbol{W}\boldsymbol{U} + \boldsymbol{F} - \boldsymbol{\xi} + \boldsymbol{\gamma} = \boldsymbol{0}$.
14: Find $\quad U_i \forall i \in \boldsymbol{S_b}, \quad \xi_i \forall i \in \boldsymbol{S_l}$, and $\gamma_i \forall i \in \boldsymbol{S_u}$.

Step 4. Decision making

15: **If** $\boldsymbol{U}, \boldsymbol{\xi}, \boldsymbol{\gamma}$ meets the KKT conditions**then**
16: Set $\boldsymbol{U}_{\text{bc}} \leftarrow \boldsymbol{U}$ and **stop**.
17: **else**
18: **Go** to step 1 with current $\boldsymbol{U}, \boldsymbol{\xi}, \boldsymbol{\gamma}$.
19: **end if**

Firstly, it is convenient to always use a center $\boldsymbol{\Theta}$ that belongs to $\bar{\mathbb{C}}_{\mathcal{H}}$. Therefore, whenever $\boldsymbol{U}_{\text{uc}} \notin \mathbb{C}_{\mathcal{H}}$ (particularly, during transients), it is proposed to bring $\boldsymbol{U}_{\text{uc}}$ on the boundary of $\mathbb{C}_{\mathcal{H}}$. This can be achieved by solving the following box-constrained quadratic programming (QP) problem, i.e.,

$$\boldsymbol{U}_{\text{bc}}(k) = \arg\min_{\boldsymbol{U}(k)} \|\boldsymbol{H}\boldsymbol{U}(k) - \bar{\boldsymbol{U}}_{\text{uc}}(k)\|_2^2 \tag{19a}$$

$$\text{subj. to:} \quad \boldsymbol{U}(k) \in \mathbb{C}_{\mathcal{H}} \subset \mathbb{R}^{\zeta} \tag{19b}$$

where a new box-constrained solution $\boldsymbol{U}_{\text{bc}} \in \mathbb{C}_{\mathcal{H}}$ is obtained by projecting $\boldsymbol{U}_{\text{uc}}$ on the boundary of $\mathbb{C}_{\mathcal{H}}$. This projection is depicted in Fig. 2 a. Here, (19b) denotes the box-constraint to the problem. Several algorithms, that may offer different computational performance, are available to solve this box-constrained QP problem [24], [25]. This work adopts an exterior point active set strategy [26]–[28], based on a Lagrangian function $\mathcal{L}$ and the Karush-Kuhn-Tucker (KKT) conditions as presented in Algorithm 2. This strategy iterates on a face of the feasible box (*Convex-Hull* $\mathbb{C}_{\mathcal{H}}$ in (18)) until either a minimizer of the objective function on that face or a point on the boundary of that face is reached. Considering the QP problem in (19), the associated Lagrangian function $\mathcal{L}$ is constructed in line 1 of Algorithm 2, where the bound constraint for $\boldsymbol{U}$ is defined as per (18), and $\boldsymbol{\xi}$ and $\boldsymbol{\gamma}$ are referred to as Lagrange multipliers. Then, the necessary KKT conditions at minimum $\boldsymbol{U}_{\text{bc}}, \boldsymbol{\xi}_{\text{bc}}, \boldsymbol{\gamma}_{\text{bc}}$ are stated in lines 2 to 6. A solution to the aforementioned system can be obtained through the four steps described in Algorithm 2. In step 1, three different sets $\boldsymbol{S_l}$, $\boldsymbol{S_u}$, and $\boldsymbol{S_b}$ are established as stated in line 7, 8, and 9, respectively. Here, the sets contain the index information of the arguments $\boldsymbol{U}$, $\boldsymbol{\xi}$, and $\boldsymbol{\gamma}$ of the Lagrangian while satisfying the conditions.

Based on these sets, the associated elements of the arguments are reset with boundary values $U_i = U_{\min,i}$, $U_i = U_{\max,i}$, $\xi_i = 0$, and $\gamma_i = 0$, see step 2.

Afterwards, the arguments are reformed by solving the linear equation stated in step 3. To this end, the linear equation can be written in a componentwise fashion as shown below

$$\sum_{j\in\mathcal{Z}} \boldsymbol{W}_{ij}\boldsymbol{U}_j + \boldsymbol{F}_i = \boldsymbol{\xi}_i - \boldsymbol{\gamma}_i, \quad \forall i \in \mathcal{Z} \tag{20}$$

As $\forall i \in \boldsymbol{S_b}$ we have that $\boldsymbol{\xi}_i = \boldsymbol{\gamma}_i = 0$, we can compute $\boldsymbol{U}_i, \forall i \in \boldsymbol{S_b}$ by splitting the sum in (20) and considering step 2 of the algorithm, i.e., $\forall i \in \boldsymbol{S_b}$,

$$\sum_{j\in\boldsymbol{S_b}} \boldsymbol{W}_{ij}\boldsymbol{U}_j = -\sum_{j\in\boldsymbol{S_l}} \boldsymbol{W}_{ij}U_{\min,j} - \sum_{j\in\boldsymbol{S_u}} \boldsymbol{W}_{ij}U_{\max,j} - \boldsymbol{F}_i. \tag{21}$$

Note that the submatrix $\boldsymbol{W}_{ij}$, with $i, j \in \boldsymbol{S_b}$ is positive definite as can be readily verified, provided that the full matrix $\boldsymbol{W}$ is positive definite. The elementary approach to find $\xi_i, \forall i \in \boldsymbol{S_l}$ and $\gamma_i, \forall i \in \boldsymbol{S_u}$ is given by

$$\xi_i = \sum_{j\in\mathcal{Z}} \boldsymbol{W}_{ij}\boldsymbol{U}_j + \boldsymbol{F}_i, \forall i \in \boldsymbol{S_l} \tag{22a}$$

$$\gamma_i = -\sum_{j\in\mathcal{Z}} \boldsymbol{W}_{ij}\boldsymbol{U}_j - \boldsymbol{F}_i, \forall i \in \boldsymbol{S_u} \tag{22b}$$

In step 4, the current solution is examined based on which the algorithm is either iterates or stops. The algorithm iterates again from step 1 with the current arguments until they satisfy the KKT conditions. Finally, the desired solution $\boldsymbol{U}_{\text{bc}} \leftarrow \boldsymbol{U}$ is obtained when the current arguments satisfy the KKT conditions, and the algorithm is stopped. Typically, it takes 10 to 20 iterations on average to complete the algorithm, which depends on the complexity of problem, e.g., length of the prediction horizon, constraints, transients, steady-state errors, etc.

Now, having $\boldsymbol{U}_{\text{bc}}$, the new ILS-problem can be written as

$$\tilde{\boldsymbol{U}}_{\text{opt}}(k) = \arg\min_{\boldsymbol{U}(k)} \|\boldsymbol{H}\boldsymbol{U}(k) - \bar{\boldsymbol{U}}_{\text{bc}}(k)\|_2^2 \tag{23}$$

Algorithm 3: Modified Initialization & SDA-Based Optimization.

function $[\boldsymbol{\Theta}, \boldsymbol{U}_{\text{ini}}, \rho_{\text{ini}}] = \textsc{Initialize}(\mathbb{C}_{\mathcal{H}})$
Compute $\boldsymbol{U}_{\text{uc}}$ as in (9)
if $\boldsymbol{U}_{\text{uc}} \in \mathbb{C}_{\mathcal{H}}$ **do**
  $\boldsymbol{\Theta} \leftarrow \bar{\boldsymbol{U}}_{\text{uc}} = \boldsymbol{H}\boldsymbol{U}_{\text{uc}}$ and $\boldsymbol{U}_{\text{ini}} \leftarrow \boldsymbol{U}_{\text{eg}}$ as in (12)
else ▷ when $\boldsymbol{U}_{\text{uc}} \notin \mathbb{C}_{\mathcal{H}}$
  Compute $\boldsymbol{U}_{\text{bc}}$ ▷ as in Algorithm 2
  $\boldsymbol{\Theta} \leftarrow \bar{\boldsymbol{U}}_{\text{bc}} = \boldsymbol{H}\boldsymbol{U}_{\text{bc}}$ and $\boldsymbol{U}_{\text{ini}} \leftarrow \boldsymbol{U}_{\text{sq}}$ as in (25)
end if
$\rho^2_{\text{ini}} \leftarrow \|\boldsymbol{H}\boldsymbol{U}_{\text{ini}} - \boldsymbol{\Theta}\|_2^2$ ▷ as in (11)
end function
Call SDA-based Optimization as in Algorithm 1
Solution: $\boldsymbol{U}_{\text{opt}}$ in (10)/ $\tilde{\boldsymbol{U}}_{\text{opt}}$ in (23) based on INITIALIZE

subject to (5d) and (5e). In (23), $\bar{\boldsymbol{U}}_{\text{bc}} = \boldsymbol{H}\boldsymbol{U}_{\text{bc}} \in \mathbb{R}^{\zeta}$ acts as a new sphere center for the SDA, i.e., $\boldsymbol{\Theta} = \bar{\boldsymbol{U}}_{\text{bc}}$; see Fig. 2 b (green square). This leads to the following optimal solution during transients

$$\tilde{\boldsymbol{U}}_{\text{opt}}(k) = [(\tilde{\boldsymbol{u}}_{\text{opt}}(k))^T \ldots (\tilde{\boldsymbol{u}}_{\text{opt}}(k+N-1))^T]^T. \tag{24}$$

Secondly, to ensure that the initial sphere remains small during transients, a new suitable initial control input sequence $\boldsymbol{U}_{\text{ini}}$ is obtained. This is calculated by quantizing each vector $\boldsymbol{u}_{\text{bc}}$ in $\boldsymbol{U}_{\text{bc}}$ to the nearest integer of $\mathbb{V}^{n_u}$ while satisfying the voltage level constraint (5e), i.e.,

$$\boldsymbol{u}_{\text{sq}}(k) = q_{\mathbb{V}}(\boldsymbol{u}_{\text{bc}}(k)) \tag{25a}$$

$$\text{subj to: } \|\Delta\boldsymbol{u}_{\text{sq}}(\ell)\|_\infty \leq 1, \forall \ell = k, \ldots, k+N\text{–}1 \tag{25b}$$

where $\Delta\boldsymbol{u}_{\text{sq}}(\ell) = \boldsymbol{u}_{\text{sq}}(\ell) - \boldsymbol{u}_{\text{sq}}(\ell-1)$ with $\boldsymbol{u}_{\text{sq}}(k-1) = \boldsymbol{u}_{\text{opt}}(k-1)$. This quantization is performed in a sequential manner starting with $\ell = k$. Thus, $\boldsymbol{u}_{\text{sq}}(k)$ will be the closest vector in $\mathbb{V}^{n_u}$ to $\boldsymbol{u}_{\text{bc}}(k)$, which satisfies $\|q_{\mathbb{V}}(\boldsymbol{u}_{\text{bc}}(k)) - \boldsymbol{u}_{\text{opt}}(k-1)\|_\infty \leq 1$. Then, this process is sequentially repeated until $\ell = k+N-1$, leading to the proposed initial control input sequence

$$\boldsymbol{U}_{\text{ini}}(k) = \boldsymbol{U}_{\text{sq}}(k) = [(\boldsymbol{u}_{\text{sq}}(k))^T \ldots (\boldsymbol{u}_{\text{sq}}(k+N-1))^T]^T. \tag{26}$$

Here, $\boldsymbol{U}_{\text{sq}} \in \mathbb{U}$ is not the standard vector quantization known as Babai estimate [29], [30] [i.e., $\boldsymbol{U}_{\text{sq}} \neq q_{\mathbb{U}}(\boldsymbol{U}_{\text{bc}})$], since $\boldsymbol{U}_{\text{sq}}$ is generated considering the voltage level constraint (25b). Notice that both $\boldsymbol{U}_{\text{sq}}$ in (25) and $\boldsymbol{U}_{\text{eg}}$ in (12) satisfy the constraints (5d) and (5e). Nevertheless, their squared Euclidean distance to the optimal solution in the transformed space formed by $\boldsymbol{H}$ can be a distinguishing feature during transients, which can be expressed as

$$\delta_{\text{sq}}(k) = \|\boldsymbol{H}\boldsymbol{U}_{\text{sq}}(k) - \boldsymbol{H}\tilde{\boldsymbol{U}}_{\text{opt}}(k)\|_2^2 \tag{27a}$$

$$\delta_{\text{eg}}(k) = \|\boldsymbol{H}\boldsymbol{U}_{\text{eg}}(k) - \boldsymbol{H}\boldsymbol{U}_{\text{opt}}(k)\|_2^2. \tag{27b}$$

As per definition in (19) and (25), $\boldsymbol{U}_{\text{sq}}$ will be in general very close to $\tilde{\boldsymbol{U}}_{\text{opt}}$, i.e., $\delta_{\text{sq}} \approx 0$. In some cases, such as in Fig. 2, $\boldsymbol{U}_{\text{sq}} = \tilde{\boldsymbol{U}}_{\text{opt}}$ and thus, $\delta_{\text{sq}} = 0$. On the contrary, $\boldsymbol{U}_{\text{eg}}$ is generally far from $\boldsymbol{U}_{\text{opt}}(k)$ in the transformed space during transients, since it depends on the previous optimal solution $\boldsymbol{U}_{\text{opt}}(k-1)$ as per (12). Comparing these two control input sequences during transients, it can be said that $\delta_{\text{sq}} \ll \delta_{\text{eg}}$. Clearly, $\boldsymbol{U}_{\text{sq}}$ ensures a significantly smaller initial sphere $\mathcal{S}_{\text{ini}}$ as per (11) than $\boldsymbol{U}_{\text{eg}}$. Therefore, $\boldsymbol{U}_{\text{sq}}$ is a better initial control input sequence during transients. Now, $\mathcal{S}_{\text{ini}} = \mathcal{S}_{\text{sq}}$ is formed using a new $\boldsymbol{\Theta} = \bar{\boldsymbol{U}}_{\text{bc}}$ and $\boldsymbol{U}_{\text{ini}} = \boldsymbol{U}_{\text{sq}}$,

$$\mathcal{S}_{\text{sq}} = \left\{\boldsymbol{U}_{\text{sq}}(k) : \rho^2_{\text{sq}}(k) = \|\boldsymbol{H}\boldsymbol{U}_{\text{sq}}(k) - \bar{\boldsymbol{U}}_{\text{bc}}(k)\|_2^2\right\}. \tag{28}$$

Notice that, during transients, $\mathcal{S}_{\text{sq}}$ is considerably smaller than $\mathcal{S}_{\text{eg}}$ in (13). Moreover, $\mathcal{S}_{\text{sq}}$ is a non-empty set which provides at least one feasible solution since $\boldsymbol{H}\boldsymbol{U}_{\text{sq}} \in \mathcal{S}_{\text{sq}}$. This situation is depicted in Fig. 2 b (green circle), where the proposed preconditioning approach provides a smaller initial circle during transients, leading to a reduced computational burden (small $\mathcal{N}_{\text{ev}}$) to obtain $\tilde{\boldsymbol{U}}_{\text{opt}}$ as per (23). It is clear from Fig. 2 that $\tilde{\boldsymbol{U}}_{\text{opt}}$ is equivalent to $\boldsymbol{U}_{\text{sq}}$ in (25) and most importantly, $\boldsymbol{U}_{\text{opt}}$ in (10) that means optimality is retained during transients. However, this situation can not be always guaranteed. Further theoretical details are given in Remark 2. Including the aforementioned preconditioning approach, a summarized pseudocode is shown in Algorithm 3 that highlights the initialization of SDA based on the *Convex-Hull* $\mathbb{C}_{\mathcal{H}}$. Once the initialization is completed, Algorithm 1 is called to find the solution $\boldsymbol{U}_{\text{opt}}$ in (10) or $\tilde{\boldsymbol{U}}_{\text{opt}}$ in (23).

Remark 1: It is important to emphasize that the key factor in the proposed preconditioning approach, that greatly reduces the computational complexity of the SDA during transients, is the idea of projecting the infeasible unconstrained optimal solution $\boldsymbol{U}_{\text{uc}} \notin \mathbb{C}_{\mathcal{H}}$ on the *Convex-Hull* $\mathbb{C}_{\mathcal{H}}$ of the original FCS $\mathbb{U}$. This can be achieved by solving (19) by any efficient box-constrained QP algorithm (e.g., exterior point active set). This key idea can be used in any multistep MPC strategy for power converters that uses SDA to efficiently find the optimal solution, including other multilevel topologies and applications, e.g., electrical drives [13].

Remark 2: For adopting the SDA in a multistep MPC problem, the original optimization problem (5) is transformed into an ILS-problem (10). Note that both optimal problems are equivalent, i.e., solving (10) will provide the same optimal solution as minimizing (5). Nevertheless, when using the proposed preconditioning approach during transient operations (i.e., $\boldsymbol{U}_{\text{uc}} \notin \mathbb{C}_{\mathcal{H}}$), the SDA solves an alternative optimization problem in (23), which in general is not equivalent to solving (10) or (5). Consequently, even though it can be ensured that the SDA will find the optimal solution, $\tilde{\boldsymbol{U}}_{\text{opt}}$, for (23), it may be only a sub-optimal solution for the original problem (5), i.e., $\tilde{\boldsymbol{U}}_{\text{opt}} \neq \boldsymbol{U}_{\text{opt}}$. Therefore, it is important to have a measure of optimality to know the closeness of the sub-optimal solution to the optimal one during transients. As analyzed in [13] and [31], because of the geometry of the optimal control problem under transients and the box constrained QP problem with *Convex-Hull*, multistep MPC may lead to only a minor loss of optimality. This work explores the cost value for the obtained solution which is indeed a standard metric of optimality (or

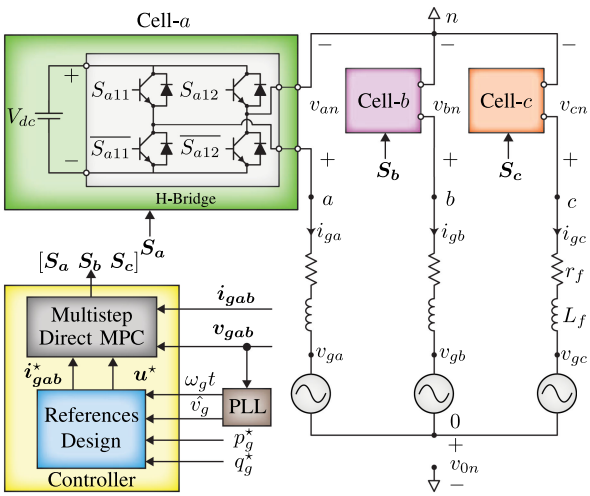

FIGURE 3. Circuit schematic of three-level H-Bridge inverter and simplified block diagram of the control scheme.

sub-optimality). Now, the cost values for the control input sequence obtained by the SDA with standard and proposed preconditioning approach can be expressed as per below

$$J_{\text{opt}}(k) = J(\boldsymbol{U}_{\text{opt}}(k)) \tag{29}$$

$$J_{\text{sopt}}(k) = \begin{cases} J_{\text{opt}}(k); & \text{when } \boldsymbol{U}_{\text{uc}} \in \mathbb{C}_{\mathcal{H}} \\ J(\tilde{\boldsymbol{U}}_{\text{opt}}(k)); & \text{when } \boldsymbol{U}_{\text{uc}} \notin \mathbb{C}_{\mathcal{H}} \end{cases}. \tag{30}$$

Here, J_{opt} is the convex quadratic form of $\boldsymbol{U}_{\text{opt}}$ as per definition in (6) for J. Note that this cost function is an equivalent form of the original one in (3). During the steady-state, i.e., generally, $\boldsymbol{U}_{\text{uc}} \in \mathbb{C}_{\mathcal{H}}$, $J_{\text{sopt}} = J_{\text{opt}}$, since the optimization problem (10) is in use at that time. Discrepancy in the cost values such as $J_{\text{sopt}} > J_{\text{opt}}$ may occur, when $\boldsymbol{U}_{\text{uc}} \notin \mathbb{C}_{\mathcal{H}}$ and a sub-optimal solution[3] (i.e., $\tilde{\boldsymbol{U}}_{\text{opt}} \neq \boldsymbol{U}_{\text{opt}}$) is obtained by solving (23). Nevertheless, $J_{\text{sopt}} = J_{\text{opt}}$, when $\tilde{\boldsymbol{U}}_{\text{opt}}$ is exactly equivalent to $\boldsymbol{U}_{\text{opt}}$. Based on the theoretical aspect stated above, an optimality analysis will be carried out in Section VII-A3 for a selected case study.

VI. CASE STUDY: GRID-CONNECTED HB-CONVERTER

In this work, a grid-connected three-phase three-level HB converter is considered as a case study based on the available laboratory resources, see Fig. 3. Thus, the selected converter model can be represented by a linear model with quantized control input (e.g., power switches, voltage levels) in order to apply the multistep MPC with proposed preconditioning approach. Note that the converter presents the same complexity as a three-level neutral-point-clamped (NPC) converter as in [3], when discarding the dc-link capacitor voltage balancing.[4] The discrete-time model and the optimal control problem of the system are presented in this section, which is the foundation to adopt the multistep MPC scheme using the SDA with standard initialization and/ or proposed preconditioning approach.

A. DISCRETE-TIME STATE-SPACE MODEL

A continuous-time dynamic model of the system for each grid-current i_{ga}, i_{gb} and grid-voltage v_{ga}, v_{gb} related to phase a and b, is given by

$$\frac{di_{ga}(t)}{dt} = -\frac{r_f}{L_f} i_{ga}(t) + \frac{1}{L_f}(v_{an}(t) - v_{ga}(t) - v_{0n}(t)) \tag{31a}$$

$$\frac{di_{gb}(t)}{dt} = -\frac{r_f}{L_f} i_{gb}(t) + \frac{1}{L_f}(v_{bn}(t) - v_{gb}(t) - v_{0n}(t)) \tag{31b}$$

$$\frac{dv_{ga}(t)}{dt} = -\frac{\omega_g}{\sqrt{3}} v_{gb}(t) + \frac{\omega_g}{\sqrt{3}} v_{gc}(t) \tag{31c}$$

$$\frac{dv_{gb}(t)}{dt} = -\frac{\omega_g}{\sqrt{3}} v_{gc}(t) + \frac{\omega_g}{\sqrt{3}} v_{ga}(t) \tag{31d}$$

where $i_{gc} = -i_{ga} - i_{gb}$, and $v_{gc} = -v_{ga} - v_{gb}$. Here, L_f is the filter inductance while r_f is its associated resistance. Here, $\omega_g = 2\pi f_g$ with f_g as the grid frequency. Additionally, for each phase $\chi = \{a, b, c\}$, the converter output voltage is represented by $v_{\chi n}(t) = V_{dc}\mu_\chi(t)$, where V_{dc} is the voltage of its isolated DC-source, and $\mu_\chi \in \mathbb{V} = \{-1, 0, 1\}$ is the output voltage level of phase χ. Furthermore, v_{0n} denotes the so-called CMV which is given by

$$v_{0n}(t) = \frac{1}{3}(v_{an}(t) + v_{bn}(t) + v_{cn}(t)). \tag{32}$$

Now, the system states, control inputs, and outputs to be controlled at any instant k are chosen as

$$\boldsymbol{x}(k) = [i_{ga}(k) \quad i_{gb}(k) \quad v_{ga}(k) \quad v_{gb}(k)]^T \in \mathbb{R}^4 \tag{33a}$$

$$\boldsymbol{u}(k) = [\mu_a(k) \quad \mu_b(k) \quad \mu_c(k)]^T \in \mathbb{V}^3 \tag{33b}$$

$$\boldsymbol{y}(k) = \boldsymbol{i_{gab}}(k) = [i_{ga}(k) \quad i_{gb}(k)]^T \in \mathbb{R}^2. \tag{33c}$$

Finally, by applying the forward Euler discretization to (31), for a sampling time T_s, a discrete-time model of the grid-connected power converter, in a form of (1), is obtained with

$$\boldsymbol{A} = \begin{bmatrix} 1 - \frac{r_f T_s}{L_f} & 0 & -\frac{T_s}{L_f} & 0 \\ 0 & 1 - \frac{r_f T_s}{L_f} & 0 & -\frac{T_s}{L_f} \\ 0 & 0 & 1 - \frac{T_s \omega_g}{\sqrt{3}} & -\frac{2T_s\omega_g}{\sqrt{3}} \\ 0 & 0 & \frac{2T_s\omega_g}{\sqrt{3}} & 1 + \frac{T_s\omega_g}{\sqrt{3}} \end{bmatrix}$$

$$\boldsymbol{B} = \frac{V_{dc}T_s}{3L_f}\begin{bmatrix} 2 & -1 & -1 \\ -1 & 2 & -1 \\ 0 & 0 & 0 \\ 0 & 0 & 0 \end{bmatrix}, \quad \boldsymbol{C} = \begin{bmatrix} 1 & 0 & 0 & 0 \\ 0 & 1 & 0 & 0 \end{bmatrix}. \tag{34}$$

[3]The cost value for any sub-optimal solution is higher than the optimal solution for the same state vector.

[4]In [32] the NPC converter represents nonlinearities for the dc-link capacitor voltage balancing, and the model is linearized at each sampling instant around the operating point.

B. OPTIMAL CONTROL PROBLEM

To implement the current control strategy, the main control objective is to track the output current references while reducing the resulting CMV. A simplified block diagram of the control scheme is shown in Fig. 3. The references are generated with the phase angle $\omega_g t$ and amplitude $\hat{v}_g$ of $v_{g\chi}$ from a phase-locked loop (PLL). Furthermore, the active ($p_g^\star$) and reactive power ($q_g^\star$) references are also provided. The typical equation of grid voltage $v_{g\chi}$ can be written as

$$v_{g\chi}(t) = \hat{v}_g \sin(\omega_g t + \phi_\chi) \tag{35}$$

Thus, the general expression for the output current references $i_{g\chi}^\star$ is given by

$$i_{g\chi}^\star(t) = \hat{i}_g \sin(\omega_g t + \phi_\chi + \phi^\star) \tag{36}$$

with the grid-current amplitude $\hat{i}_g = \frac{2s_g^\star}{3\hat{v}_g}$ where $s_g^\star = \sqrt{p_g^{\star 2} + q_g^{\star 2}}$ is the apparent power reference and the phase displacement angle is $\phi^\star = \cos^{-1}\frac{p_g^\star}{s_g^\star}$, between $v_{g\chi}$ and $i_{g\chi}$. Moreover, $\phi_a = 0$, $\phi_b = -\frac{2\pi}{3}$, and $\phi_c = +\frac{2\pi}{3}$. Thus, $\boldsymbol{y}^\star = \boldsymbol{i_{gab}}^\star = [i_{ga}^\star \quad i_{gb}^\star]^T$ is chosen for $\boldsymbol{y}$ in (33c). Then, as per [19], the CMV can be minimized by tracking the control-input references in $\boldsymbol{u}^\star = [v_{\ell a}^\star \quad v_{\ell b}^\star \quad v_{\ell c}^\star]$, for

$$v_{\ell\chi}^\star(t) = \frac{1}{V_{dc}}\left\{r_f i_{g\chi}^\star(t) + L_f \frac{di_{g\chi}^\star(t)}{dt} + v_{g\chi}(t)\right\}. \tag{37}$$

Finally, the optimal control input sequence $\boldsymbol{U}_{\text{opt}}$ is obtained by solving the original optimization problem in (5). Then, based on $\boldsymbol{u}_{\text{opt}}$ (first element of $\boldsymbol{U}_{\text{opt}}$), the states of power switches, $\boldsymbol{S_\chi} = [S_{\chi 11}, S_{\chi 12}, \overline{S_{\chi 11}}, \overline{S_{\chi 12}}]$, are found by applying a sorting algorithm for equal utilization of power switches [21].

VII. RESULTS

This section evaluates the effectiveness and the computational performance of the proposed SDA preconditioning approach by using the PIL simulations and conducting experiments. The analysis and results presented in this section are focused on the computational improvements and practical benefits of the preconditioning approach during transients. As a measure of comparison, the maximum values of the computational metrics ρ_{ini}, $\mathcal{N}_{\text{ev}}$ and T_e are investigated for both the standard SDA initialization and proposed preconditioning approach. The system parameters are shown in Table 1. Throughout this section, all results are obtained under a transient test condition (TTC_1), when a positive step change in $s_g^\star$ is applied from 0.45 p.u. to 1 p.u., i.e.:

$$TTC_1 : s_g^\star = \begin{cases} p_g^\star = 0.45 \text{ p.u. } \& \ q_g^\star = 0.00 \text{ p.u.} \\ p_g^\star = 0.89 \text{ p.u. } \& \ q_g^\star = 0.45 \text{ p.u.} \end{cases}. \tag{38}$$

A. PIL-SIMULATION RESULTS

A key parameter of the multistep MPC strategy is the prediction horizon N. In a real implementation, this has to be designed not only to improve the closed-loop performance but also to keep the required computational burden within a feasible limit, i.e., $T_e < T_s$. In this work, the design of N is performed with the aid of PIL-simulations. Here, the system is simulated in a PC with MATLAB-Simulink, while the controller is executed in real-time in a dSPACE DS1006, as shown in Fig. 4. Note that the well-known time-delay compensation [33] is included in the control formulation.

TABLE I **Main System Parameters and Controller Settings for Simulation and Experimental Tests**

Parameter	Symbol	SI value	p.u. value
dc voltage supply per HB	V_{dc}	180 V	1.025
Grid apparent power	S_g	2.24 kVA	1.000
Grid line-to-line voltage	V_g	215 V	1.225
Grid current	I_g	6.005 A	0.707
Grid frequency	f_g	50 Hz	1.000
Filter resistance	r_f	0.5 Ω	0.024
Filter inductance	L_f	7 mH	0.106
Weighting factor	σ	10^{-6}	—
Sampling frequency	f_s	5 kHz	—

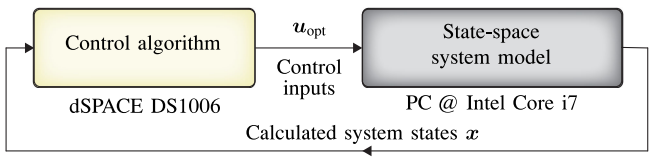

FIGURE 4. **Block diagram of the PIL-simulation.**

Instead of reading the actual measurements from the power converter, the system states $\boldsymbol{x}(k)$ are obtained (not in real-time) from the simulator. Then, based on these virtual measurements, the dSPACE system computes the optimal control input $\boldsymbol{u}_{\text{opt}}$ in real-time. Finally, this optimal input is implemented in the simulation to obtain, thus, a new system state in the next sampling interval. At every stage, the execution time T_e required by the controller to obtain an optimal input is recorded by the available function (*'turnaroundTime'*) in the control platform. This procedure allows one to safely evaluate T_e for different prediction horizons during both steady-state and transients.

1) Selection of Prediction Horizon *N*

As a baseline, the PIL simulations are carried out for $N \in [1, 10]$ and under the TTC_1 in (38), when the converter is governed by a multistep direct MPC with the *standard SDA initialization*. Then, the maximum values of the metrics denoted as $\widehat{\rho}_{\text{ini}}$, $\widehat{\mathcal{N}}_{\text{ev}}$, and $\widehat{T}_e$, are recorded for both steady-state (SS) and transient-state (TS). The results are presented in semi-logarithmic bar-plots in Fig. 5. It is possible to see that all the metrics for TS are consistently higher than the ones for SS. According to Fig. 5 c, $\widehat{T}_e$ exceeds the sampling interval limit, $T_s = 1/f_s = 200\mu s$, for $N > 3$ during transients. Fig. 6 shows the computational performance of the SDA working with the proposed preconditioning approach, which is obtained for the same test conditions. As one can see, all the metrics for TS

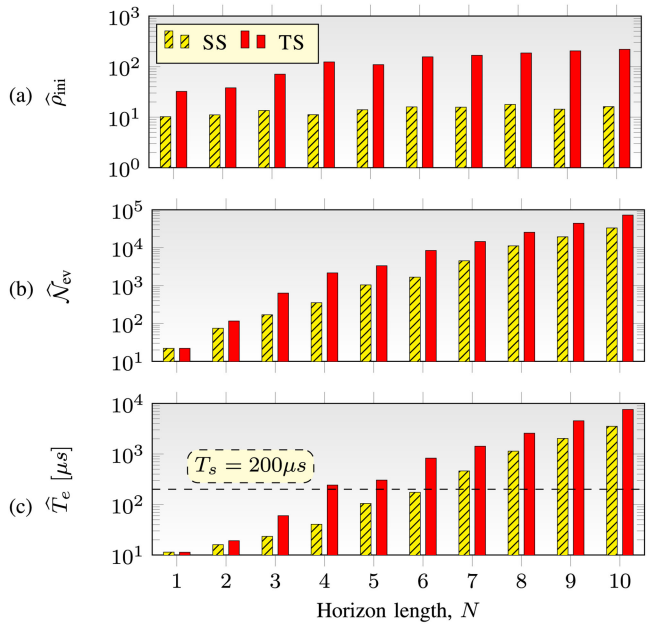

FIGURE 5. PIL-simulation based computational performance of multistep MPC considering the *standard SDA initialization* under TTC_1. For $N \in [1, 10]$, the results in steady-state (*SS*) and transient-state (*TS*) are in semi-logarithmic bar-plots. (a) maximum initial radius $\widehat{\rho}_{\text{ini}}$, (b) maximum number of evaluated nodes $\widehat{\mathcal{N}}_{\text{ev}}$, and (c) maximum execution time $\widehat{T}_e$.

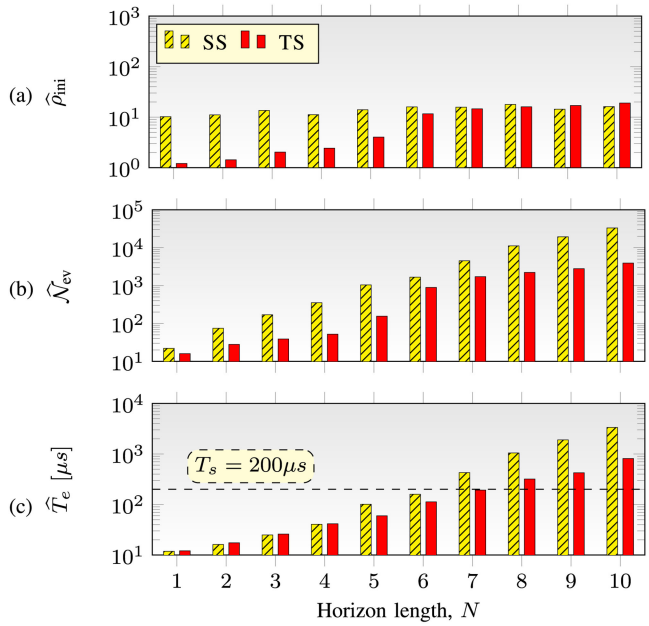

FIGURE 6. PIL-simulation based computational performance of multistep MPC considering the *proposed SDA preconditioning approach* under TTC_1. For $N \in [1, 10]$, the results in steady-state (SS) and transient-state (TS) are in semi-logarithmic bar-plots. (a) maximum initial radius $\widehat{\rho}_{\text{ini}}$, (b) maximum number of evaluated nodes $\widehat{\mathcal{N}}_{\text{ev}}$, and (c) maximum execution time $\widehat{T}_e$.

are significantly reduced in comparison with Fig. 5, while the results for SS are unaffected. For the case of $N = 6$ and TS, $\widehat{\rho}_{\text{ini}}$ is drastically reduced from 156.65 to 11.66. Furthermore, $\widehat{\mathcal{N}}_{\text{ev}}$ and $\widehat{T}_e$ are also significantly reduced from 8464 and 826.7μs to 1667 and 159.73μs, respectively. Importantly, $\widehat{T}_e$ in Fig. 6 c is within the sampling interval limit ($\widehat{T}_e < T_s$) for $N \leq 6$. Hence, the proposed preconditioning approach allows one, in this case, to carry out a real-time implementation of multistep MPC with a prediction horizon that is twice as large as in the standard implementation. It is important to highlight that going from $N = 3$ to 6, the optimal solution has to be found from a set of input combinations that increases from $27^3 \approx 10^{4.29}$ to $27^6 \approx 10^{8.59}$.

2) Performance Evaluation

Firstly, the multistep MPC closed-loop performance under TTC_1, tuned with the chosen $N = 6$ and considering the proposed preconditioning approach, is presented in Fig. 7. The close view of each computational metric is also presented in Fig. 7(d)-(f) for the time span 25 − 35 ms. Here, the computational metrics, i.e., initial radius ρ_{ini}, number of evaluated nodes $\mathcal{N}_{\text{ev}}$ and execution time T_e, are not increased drastically during the transient compared to steady-state operation, see Fig. 7(d)-(f), respectively. In particular, T_e is less than the sampling interval limit during the whole converter operation, i.e., $T_e < T_s$. This ensures that the control problem is solved to optimality, see Fig. 7(f). In this case, an average value of the semiconductor device switching frequency of $\tilde{f}_{sw} = 380$ Hz is observed, when the system is operating in steady-state with its full power rating. Secondly, the same test scenario is simulated considering the standard initialization approach of the SDA. The results are displayed for 20-40 ms in the left-hand column of Fig. 8. The system performance [p_g, q_g, $\boldsymbol{i}_{gabc}$ and $\boldsymbol{v}_{abcn}$ in the left-hand column of Fig. 8(a)-(c), respectively] is similar to the one presented in Fig. 7. However, ρ_{ini} and $\mathcal{N}_{\text{ev}}$ experience an abrupt increase at 30 ms; see left-hand column of Fig. 8(d)-(e). This leads to a large execution time ($T_e = 826.7\mu$s) that exceeds the sampling interval limit during this transient, i.e., $T_e > T_s$, as can be seen from the left-hand column of Fig. 8(e). It is important to emphasize that it is only possible to obtain this result with a PIL-simulation. In a real implementation, the optimization algorithm will be stopped when the execution time meets the sampling interval, implementing the best available solution obtained, but not necessarily the optimal one. In the right-hand column of Fig. 8, a PIL-simulation is presented with the computational complexity of the SDA bounded as in [11]. Here, limited number of computations in SDA are permitted to satisfy the sampling interval limit, i.e., $T_e \not> T_s$, while sub-optimal solutions may be obtained at times. To this end, the limit $\mathcal{N}_{\text{ev}}^{lm} = 1750$ is added to the SDA, which is equivalent to an allowable situation $T_e unknown.T_s$. Note that the choice of the limit $\mathcal{N}_{\text{ev}}^{lm} = 1750$ is obtained by trail-and-error using PIL-simulations, and it may only be compatible for the system under study and the computational power of dSPACE DS1006. It can be observed that the closed-loop performance during the transient is deteriorated, producing almost 90% undershoots in the active and reactive power tracking. As a consequence, the system dynamics become substandard with a transient variation of almost 90%, and a settling time of 5 ms.

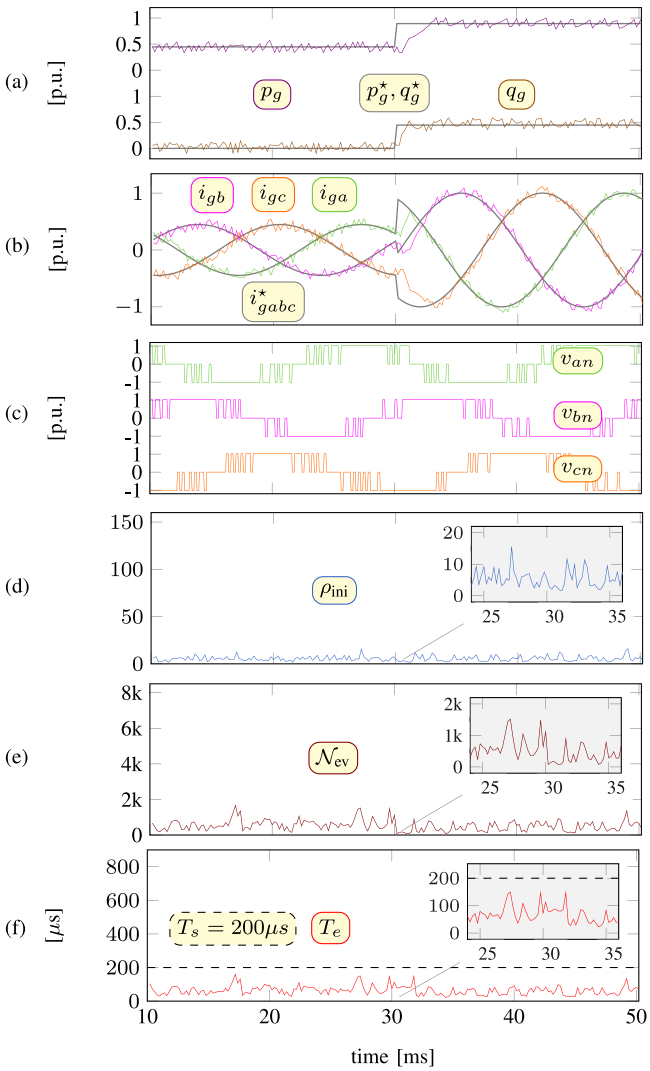

FIGURE 7. **PIL-simulation results for $N = 6$ using the *proposed SDA preconditioning approach*, under TTC_1. (a) active and reactive power p_g, q_g, (b) grid currents i_{gabc}, (c) inverter voltages v_{abcn}, (d) initial radius ρ_{ini}, (e) number of evaluated nodes $\mathcal{N}_{\text{ev}}$, and (f) execution time T_e.**

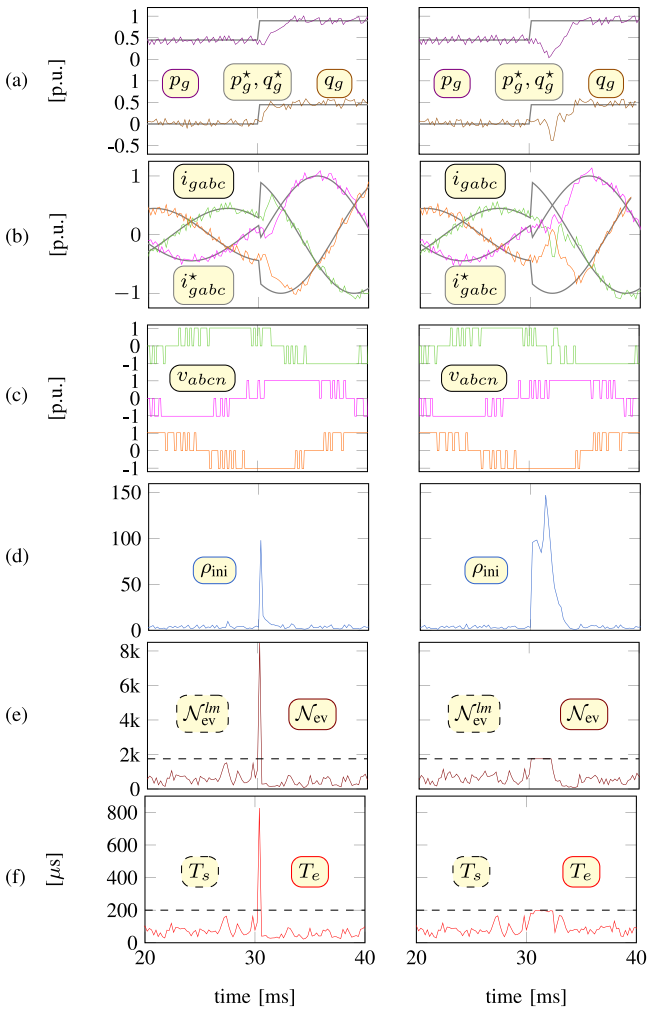

FIGURE 8. **PIL-simulation results for $N = 6$ using the standard SDA initialization, under TTC_1. (a) active and reactive power p_g, q_g, (b) grid currents i_{gabc}, (c) inverter voltages v_{abcn}, (d) initial radius ρ_{ini}, (e) number of evaluated nodes $\mathcal{N}_{\text{ev}}$, and (f) execution time T_e. The figures in right-hand column are obtained when computations are limited to $\mathcal{N}_{\text{ev}}^{lm} = 1750$ to ensure $T_e = T_s$.**

Generally, a transient variation of $\pm 20\%$ and settling time of 1.5 ms are recommended as per *IEEE-standard 1662-2016* for the design and application of power electronics in electrical power systems [34]. Clearly, the transient performance in this case violates this standard. The iterative optimization process in the SDA is designed to stop whenever the limit $\mathcal{N}_{\text{ev}}^{lm} = 1750$ is reached. In that case, the immediate incumbent solution (sub-optimal) found is applied to the system, which may differ from the optimal solution. Consequently, adding a calculation limit $\mathcal{N}_{\text{ev}}^{lm}$ may lead the SDA to only find sub-optimal solutions that can produce undesirable closed-loop performance.

3) Optimality Analysis

This section carries out an optimality analysis based on the theoretical aspect described in Remark 2. Firstly, the PIL-simulation of multistep MPC for prediction horizon $N = 6$ is run with the proposed SDA preconditioning approach under TTC_1, and the obtained solution is applied to the system accordingly. Then, the cost value J_{sopt} is computed using (30). At the same time, the SDA with standard initialization approach stated in Section III-B is also run to obtain $\boldsymbol{U}_{\text{opt}}$ by solving (10). This allows us to compute the optimal cost value J_{opt} as per (29). Note that the computations of J_{opt} and J_{sopt} use the same system information (state variables and outputs) obtained for the proposed approach. In this way, one can have a fair comparison between two cost values. The comparative results of J_{opt} and J_{sopt} are shown in Fig. 9 a. It can be observed that the cost values are equal for the whole converter operation periods, i.e., $J_{\text{sopt}} = J_{\text{opt}}$. This is generally expected for steady-state operation, since both methods are solving the same optimization problem (10). Most importantly, the proposed one is capable of ensuring that the optimal solution is found during the transient at 30 ms, i.e., $\widetilde{\boldsymbol{U}}_{\text{opt}} = \boldsymbol{U}_{\text{opt}}$ and $J_{\text{sopt}} = J_{\text{opt}}$, as can be seen

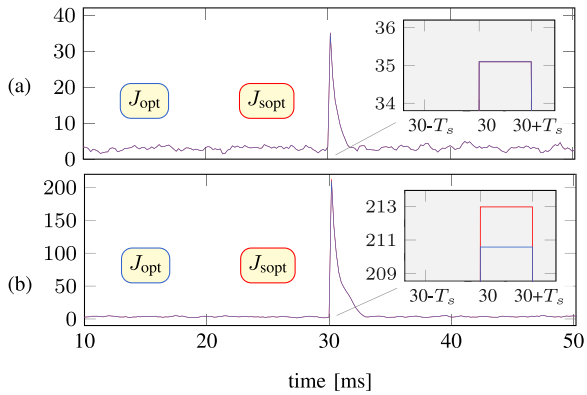

FIGURE 9. The optimality analysis of the multistep MPC using standard initialization and proposed preconditioning approach for $N = 6$, under two different test conditions: (a) TTC_1 and (b) TTC_2.

from the close view. However, this optimality can not be guaranteed always from a theoretical perspective. There may exist different systems, transient test conditions, operation points, for which optimality may be violated at certain times with the proposed preconditioning approach.

To investigate this further, the optimality analysis mentioned above has been performed under a new transient test condition TTC_2 given below:

$$\mathrm{TTC}_2 : s_g^\star = \begin{cases} p_g^\star = 0.045 \text{ p.u. } \& \ q_g^\star = -0.45 \text{ p.u.} \\ p_g^\star = 0.89 \text{ p.u. } \& \ q_g^\star = +0.45 \text{ p.u.} \end{cases} . \quad (39)$$

The corresponding cost values J_{opt} and J_{sopt} are shown in Fig. 9 b. It can be observed that both plots are identical for the whole operation of the converter, i.e., $J_{\text{sopt}} = J_{\text{opt}}$, except for the transient at 30 ms. From the close view, it is clear that $J_{\text{sopt}} > J_{\text{opt}}$, which is an increment of 1.12% only. Thus, a sub-optimal solution $\tilde{\boldsymbol{U}}_{\text{opt}} \neq \boldsymbol{U}_{\text{opt}}$ is applied to the system only at 30 ms. In other words, the obtained sub-optimal solution is 98.88% close to the optimal one.

To conclude, even though the proposed preconditioning approach allows one to reduce the computational burden during transients, optimality in the control input sequence can not be always guaranteed. This occasional small loss in optimality can be traded in for a considerable reduction in the computational burden during transients. Surely, theoretical optimality analysis emerges as an open problem for subsequent research.

B. EXPERIMENTAL RESULTS

The experimental performance of the multistep MPC with the proposed preconditioning strategy for $N = 6$ is presented in Fig. 10 under the same test scenario TTC_1 maintained for the PIL-simulation. Here, the close view of each computational metric is also presented for the time span $25 - 35$ ms, see Fig. 10(d)-(f). The control algorithm was implemented in the same dSPACE DS1006 while the switching states of the power converter were generated in an FPGA module DS5203. As expected, the closed-loop performance (Fig. 10(b)-(c)) and the computational performance (Fig. 10(d)-(f)) are similar to

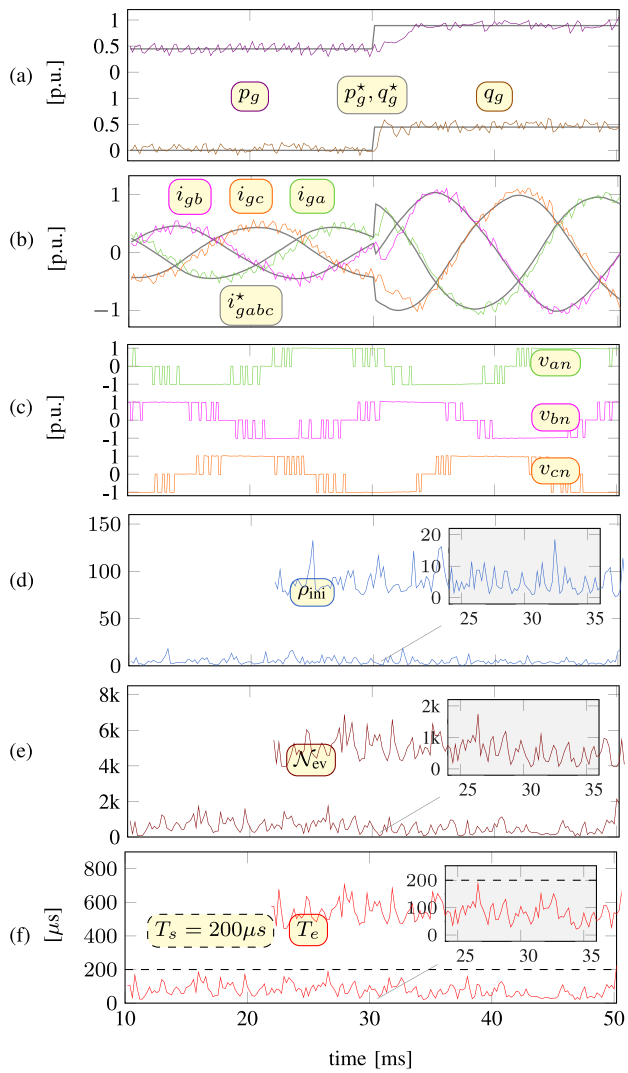

FIGURE 10. Experimental results for $N = 6$ using the *proposed SDA preconditioning approach*, under TTC_1. (a) active and reactive power p_g, q_g, (b) grid currents i_{gabc}, (c) inverter voltages v_{abcn}, (d) initial radius ρ_{ini}, (e) number of evaluated nodes $\mathcal{N}_{\text{ev}}$, and (f) execution time T_e.

the PIL simulation results in Fig. 7. Importantly, it can be observed from Fig. 10(f) that the condition $T_e < T_s$ is satisfied during both steady-state and transient operation, which ensures the safe and optimal operation of the power converter.

VIII. CONCLUSION

A crucial computational burden problem that arises due to the transient operation of power converters when using multistep MPC has been addressed in this work. This problem has been solved by proposing a preconditioning approach, which provides a suitable initial sphere for the sphere decoding algorithm in order to efficiently find the solution. A case study with processor-in-the-loop simulations and experimental results has been conducted to confirm the feasibility and effectiveness of the proposal in practical applications such as grid-connected converters operating at very low semiconductor switching frequencies, e.g., below 450 Hz. The

computational performance showed that a small number of candidate solutions is evaluated during transients, thus the computational burden is drastically reduced in comparison with the standard SDA initialization. Most importantly, the proposed preconditioning approach allows one to achieve real-time implementation up to a prediction horizon of six. In contrast, the standard SDA is restricted to the prediction horizon three with comparable technology. Nevertheless, optimality in the control input sequence cannot always be guaranteed, since an alternative optimization problem is solved by the SDA during transients. For this case, a very small degree of sub-optimality appears in some particular transients. This occasional small loss in optimality can be traded for a significant reduction in the computational burden during transients. In general, the chance of obtaining sub-optimality case depends on the aggressiveness of transients and also on the system types. This topic itself demands an extensive in depth analysis, and is the scope of future research. Further results showed that if this computational burden problem is not properly addressed, the system may have an undesirable transient behavior, which clearly demonstrates the practical benefit of the proposal. Consequently, the proposed preconditioning approach enables multistep direct MPC based on the SDA to work in the whole operational range of a power converter becoming, thus, a viable control alternative. Moreover, due to its generality, the proposed preconditioning approach can be used in any multistep direct MPC strategy for medium/ high-power converters that use the SDA, including other multilevel topologies and applications, e.g., medium/ high-power electrical drives.

REFERENCES

[1] J. Rodríguez *et al.*, "State of the art of finite control set model predictive control in power electronics," *IEEE Trans. Ind. Inform.*, vol. 9, no. 2, pp. 1003–1016, May 2013.

[2] H. Vikalo and B. Hassibi, "On the sphere-decoding algorithm ii. generalizations, second-order statistics, and applications to communications," *IEEE Trans. Signal Process.*, vol. 53, no. 8, pp. 2819–2834, Aug. 2005.

[3] T. Geyer and D. E. Quevedo, "Multistep finite control set model predictive control for power electronics," *IEEE Trans. Power Electron.*, vol. 29, no. 12, pp. 6836–6846, Dec. 2014.

[4] T. Geyer and D. E. Quevedo, "Performance of multistep finite control set model predictive control for power electronics," *IEEE Trans. Power Electron.*, vol. 30, no. 3, pp. 1633–1644, Mar. 2015.

[5] S. Fuchs, M. Jeong, and J. Biela, "Long horizon, quadratic programming based model predictive control (MPC) for grid connected modular multilevel converters (MMC)," in *Proc. IECON 45th Annu. Conf. IEEE Ind. Electron. Soc.*, 2019, vol. 1, pp. 1805–1812.

[6] A. Andersson and T. Thiringer, "Assessment of an improved finite control set model predictive current controller for automotive propulsion applications," *IEEE Trans. Ind. Electron.*, vol. 67, no. 1, pp. 91–100, Jan. 2020, DOI 10.1109/TIE.2019.2898603.

[7] Zheng Hu, Qian Liu, and K. Hameyer, "A study of multistep model predictive direct current control for dynamic drive applications with high switching frequency," in *Proc. 8th IET Int. Conf. Power Electron., Mach. Drives*, DOI 10.1049/cp.2016.0354, Apr. 2016, pp. 1–6.

[8] X. W. Chang, J. Wen, and X. Xie, "Effects of the lll reduction on the success probability of the babai point and on the complexity of sphere decoding," *IEEE Trans. Inf. Theory*, vol. 59, no. 8, pp. 4915–4926, Aug. 2013.

[9] A. K. Lenstra, H. W. Lenstra, and Jr, and L. Lovász, "Factoring polynomials with rational coefficient," *Math. Ann.*, vol. 261, no. 4, pp. 515–534, 1982.

[10] P. Karamanakos, T. Geyer, and R. Kennel, "A computationally efficient model predictive control strategy for linear systems with integer inputs," *IEEE Trans. Control Syst. Technol.*, vol. 24, no. 4, pp. 1463–1471, Jul. 2016.

[11] P. Karamanakos, T. Geyer, and R. Kennel, "Suboptimal search strategies with bounded computational complexity to solve long-horizon direct model predictive control problems," in *Proc. IEEE Energy Convers. Congr. Expo.*, Sep. 2015, pp. 334–341.

[12] R. Baidya *et al.*, "Fast multistep finite control set model predictive control for transient operation of power converter," in *Proc. Ind. Electron. Soc., IECON 42nd Annu. Conf.*, Oct. 2016, pp. 5039–5045.

[13] P. Karamanakos, T. Geyer, and R. P. Aguilera, "Computationally efficient long-horizon direct model predictive control for transient operation," in *Proc. IEEE Energy Convers. Congr. Expo.*, Oct. 2017, pp. 4642–4649.

[14] P. Acuna, C. A. Rojas, R. Baidya, R. P. Aguilera, and J. E. Fletcher, "On the impact of transients on multistep model predictive control for medium-voltage drives," *IEEE Trans. Power Electron.*, vol. 34, no. 9, pp. 8342–8355, Sep. 2019.

[15] P. Cortés, A. Wilson, S. Kouro, and J. Rodríguez, and Abu-Rub,, "Model predictive control of multilevel cascaded H-Bridge inverters," *IEEE Trans. Ind. Electron.*, vol. 57, no. 8, pp. 2691–2699, 2010.

[16] R. Vargas, P. Cortes, U. Ammann, J. Rodriguez, and J. Pontt, "Predictive control of a three-phase neutral-point-clamped inverter," *IEEE Trans. Ind. Electron.*, vol. 54, no. 5, pp. 2697–2705, Oct. 2007.

[17] H. Gao, B. Wu, D. Xu, M. Pande, and R. P. Aguilera, "Common-mode voltage reduced model predictive control scheme for current source converter-fed induction motor drives," *IEEE Trans. Power Electron.*, vol. 32, no. 6, pp. 4891-4904, Jun. 2017.

[18] P. Cortés, J. Rodríguez, D. E. Quevedo, and C. Silva, "Predictive current control strategy with imposed load current spectrum," *IEEE Trans. Power Electron.*, vol. 23, no. 2, pp. 612–618, Mar. 2008.

[19] R. Baidya, R. P. Aguilera, P. Acuna, S. Vazquez, and H. du Toit Mouton, "multistep model predictive control for cascaded H-Bridge inverters: Formulation and analysis," *IEEE Trans. Power Electron.*, vol. 33, no. 1, pp. 876–886, Jan. 2018.

[20] R. P. Aguilera and D. E. Quevedo, "Predictive control of power converters: Designs with guaranteed performance," *IEEE Trans. Ind. Inform.*, vol. 11, no. 1, pp. 53–63, Feb. 2015.

[21] R. P. Aguilera *et al.*, "Predictive control of cascaded h-bridge converters under unbalanced power generation," *IEEE Trans. Ind. Electron.*, vol. 64, no. 1, pp. 4–13, Jan. 2017.

[22] R. P. Aguilera *et al.*, "Selective harmonic elimination model predictive control for multilevel power converters," *IEEE Trans. Power Electron.*, vol. 32, no. 3, pp. 2416–2426, Mar. 2017.

[23] R. B. Schnabel and E. Eskow, "A new modified cholesky factorization," *SIAM J. Scientific. Stat. Comput.*, vol. 11, no. 6, pp. 1136–1158, 1990.

[24] S. Bubeck, *Convex Optimization: Algorithms and Complexity*. Now Foundations and Trends, 2015.

[25] S. Boyd and L. Vandenberghe, *Convex Optimization*. Cambridge, UK: Cambridge Univ. Press, 2004.

[26] J. J. Moré and G. Toraldo, "Algorithms for bound constrained quadratic programming problems," *Numerische Mathematik*, vol. 55, no. 4, pp. 377–400, 1989.

[27] J. J. Moré and G. Toraldo, "On the solution of large quadratic programming problems with bound constraints," *SIAM J. Optim.*, vol. 1, no. 1, pp. 93–113, 1991.

[28] P. E. Gill, W. Murray, and M. A. Saunders, "Snopt: An sqp algorithm for large-scale constrained optimization," *SIAM Rev.*, vol. 47, no. 1, pp. 99–131, 2005.

[29] L. Babai, "On lovász lattice reduction and the nearest lattice point problem," *Combinatorica*, vol. 6, no. 1, pp. 1–13, 1986.

[30] J. Wen and X. W. Chang, "Success probability of the babai estimators for box-constrained integer linear models," *IEEE Trans. Inf. Theory*, vol. 63, no. 1, pp. 631-648, Jan. 2017.

[31] R. Baidya *et al.*, "Dealing with suboptimality in multistep model predictive control for transient operations," in *Proc. IEEE Energy Convers. Congr. Expo.*, 2019, pp. 3780–3785.

[32] E. Liegmann, P. Karamanakos, T. Geyer, T. Mouton, and R. Kennel, "Long-horizon direct model predictive control with active balancing of the neutral point potential," in *Proc. IEEE Int. Symp. Predictive Control Elect. Drives Power Electron.*, 2017, pp. 89–94.

[33] P. Cortes, J. Rodriguez, C. Silva, and A. Flores, "Delay compensation in model predictive current control of a three-phase inverter," *IEEE Trans. Ind. Electron.*, vol. 59, no. 2, pp. 1323–1325, Feb. 2012.

[34] "IEEE Recommended Practice for the Design and Application of Power Electronics in Electrical Power Systems," *IEEE Std 1662-2016 (Revision IEEE Std 1662-2008)*, pp. 1–68, Mar. 2017.

ROKY BAIDYA (Member, IEEE) received the B.Sc. degree in electrical and electronic engineering from the Chittagong University of Engineering and Technology (CUET), Chittagong, Bangladesh, and the Ph.D. degree in electrical engineering from the University of New South Wales (UNSW), Sydney, Australia, in 2011 and 2018, respectively. His Ph.D. research was with the Australian Energy Research Institute under the School of Electrical Engineering and Telecommunications, UNSW.

From 2011 to 2014, and 2018 to 2020, he was with the Department of Electrical and ELectrical Engineering at CUET, as a Lecturer and an Assistant Professor, respectively. Since May 2020, he has been with the School of Electrical and Data Engineering, University of Technology Sydney, Australia, where he is currently working as a Research Support. His main research interests focus on the model predictive control of power converters and electric drives with fast optimization algorithms, renewable energy integration, and real-time simulation of Microgrids.

RICARDO P. AGUILERA (Member, IEEE) received the B.Sc. degree in electrical engineering from the Universidad de Antofagasta, Antofagasta, Chile, the M.Sc. degree in electronics engineering from the Universidad Tecnica Federico Santa Maria, Valparaíso, Chile, and the Ph.D. degree in electrical engineering from the University of Newcastle (UoN), Newcastle, NSW, Australia, in 2003, 2007, and 2012, respectively.

From 2012 to 2013, he was a Research Academic with UoN, where he was part of the Centre for Complex Dynamic Systems and Control. From 2014 to 2016, he was a Senior Research Associate with the University of New South Wales, Australia, where he was part of the Australian Energy Research Institute. Since September 2016, he has been with the School of Electrical and Data Engineering, at the University of Technology Sydney, Australia, where he currently holds a Senior Lecturer position. His main research interests include theoretical and practical aspects on model predictive control with application to power electronics, renewable energy integration, and microgrids.

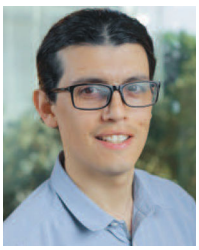

PABLO ACUÑA (Member, IEEE) received the B.Sc. degree in electronics engineering, the B.Eng. degree in electronics engineering, and the Ph.D. degree in electrical engineering from the University of Concepción, Concepción, Chile, in 2004, 2007, and 2013, respectively. From 2014 to 2017, he was a Research Associate with the University of New South Wales, Australia. From 2018 to 2019, he was Lecturer with the School of Engineering, RMIT University, Melbourne, Australia.

He is currently a Lecturer with the Department of Electrical Engineering, Universidad de Talca, Chile.

His research interests include electrical power conversion systems and their applications in industry, transportation, and utility.

TOBIAS GEYER (Senior Member, IEEE) received the Dipl.-Ing. and Ph.D. degrees in electrical engineering from ETH Zurich, Zurich, Switzerland, in 2000 and 2005, respectively, and the Habilitation degree in power electronics from ETH Zurich, Zurich, Switzerland, in 2017.

After the Ph.D., he spent three years with GE Global Research, Munich, Germany, three years with the University of Auckland, Auckland, New Zealand, and eight years with ABBs Corporate Research Centre, Baden-Dttwil, Switzerland. In 2016, he became a Senior Principal Scientist for power conversion control. He was appointed as an Extraordinary Professor at Stellenbosch University, Stellenbosch, South Africa, from 2017 to 2020. In 2020, he joined ABBs medium-voltage drives business as R&D Platform Manager of the ACS6000/6080.

He is the author of 35 patent families and the book Model Predictive Control of High Power Converters and Industrial Drives (Wiley, 2016). He teaches a regular course on model predictive control at ETH Zurich. His research interests include medium-voltage and low-voltage drives, utility-scale power converters, optimized pulse patterns, and model predictive control.

Dr. Geyer was the recipient of the 2017 First Place Prize Paper Award in the Transactions on Power Electronics, the 2014 Third Place Prize Paper Award in the Transactions on Industry Applications, and of two Prize Paper Awards at conferences. He is a former Associate Editor for the *Transactions on Industry Applications* (from 2011 until 2014) and the *Transactions on Power Electronics* (from 2013 until 2019). He was an international program committee Vice Chair of the IFAC conference on Nonlinear Model Predictive Control in Madison, WI, USA, in 2018. Dr. Geyer is a Distinguished Lecturer of the Power Electronics Society in the years 2020 and 2021.

RAMÓN A. DELGADO received the professional title of Ingeniero Civil Electrónico and M.Sc. degrees in electronic engineering from Universidad Técnica Federico Santa María, Chile, in 2009. He received the Ph.D. degree in electrical engineering from the University of Newcastle, Australia, in 2014. He is currently a Research Academic with the University of Newcastle. In his current role, Dr. Delgado is mainly focused on the current collaboration project between the University of Newcastle and the Swedish company Ericsson AB. His research interests include system identification, control, signal processing, and optimisation.

DANIEL E. QUEVEDO (Senior Member, IEEE) received the Ingeniero Civil Electrónico and M.Sc. degrees from Universidad Técnica Federico Santa María, Valparaíso, Chile, in 2000, and 2005, respectively, and the Ph.D. degree from the University of Newcastle, Australia. He is a Professor with the School of Electrical Engineering and Robotics, Queensland University of Technology (QUT), in Australia. Before joining QUT, he established and led the Chair in Automatic Control at Paderborn University, Germany. His research interests include networked control systems, control of power converters and cyberphysical systems security. In 2003, he was a receipent of the IEEE Conference on Decision and Control Best Student Paper Award and was also a finalist in 2002. He was a co-recipient of the 2018 IEEE Transactions on Automatic Control George S. Axelby Outstanding Paper Award.

Prof. Quevedo currently is Associate Editor for the *IEEE Control Systems Magazine* and in the Editorial Board of the *International Journal of Robust and Nonlinear Control*. From 2015–2018, he was a Chair of the IEEE Control Systems Society *Technical Committee on Networks & Communication Systems*.

HENDRIK DU TOIT MOUTON (Member, IEEE) received the B.Sc., B.Sc. (Hons.), M.Sc., and Ph.D. degrees in mathematics from the University of the Orange Free State, Bloemfontein, South Africa, in 1986, 1987, 1988, and 1991, respectively, and the B.Eng. and Ph.D. degrees in electrical engineering from the University of Stellenbosch, Stellenbosch, South Africa, in 1996 and 2000, respectively. He is currently a Professor of electrical engineering with the University of Stellenbosch and Leader of the Power Electronics Research Group. He has authored and coauthored more than 130 journal and conference papers in mathematics and power electronics. His research interests include multilevel converters, modeling and control of power electronic converters, and class-D audio amplifiers.